JOURNAL OF GEOPHYSICAL RESEARCH, VOL. 95, NO. B4, PAGES 4833–4856, APRIL 10, 1990

Temperatures, Heat Flux, and Frictional Stress Near Major Thrust Faults

PETER MOLNAR[1] AND PHILIP ENGLAND

Department of Earth Sciences, Oxford University, Oxford, England

We examine the two-dimensional advective and conductive transport of heat in a region of thrust faulting. Both simple theoretical considerations and numerical experiments show that the steady state temperatures near the fault are reduced by a divisor, $S = 1 + b\sqrt{(z_f V \sin\delta)/\kappa}$ below what they would be with the same heat sources but in the absence of advection. In this expression z_f is the depth to the fault, V is the slip rate, δ is the component of the dip of the fault in the direction of underthrusting, κ is thermal diffusivity, and b is a dimensionless factor that is essentially equal to one for most forms of heating. Initial changes in temperatures near the fault are given by $T(z_f, t) = T(z_f, 0) - \frac{1}{2} V \sin\delta \partial T(z, 0)/\partial z$. These simple formulae are successful because of the neglible influence of lateral conduction of heat, at least for slip rates of a few mm/yr or more. Two time constants govern the transition from the initial change in temperature to steady state: $t_1 = u_f/V$, where u_f is the distance along the fault in the direction of underthrusting from the surface to the depth in question, and $t_2 = z_f^2/\kappa\pi^2$, where z_f is the depth to the fault. When elapsed times exceed the sum of these two time constants, temperatures differ from their steady state values by only about 10 percent. The numerical experiments indicate that the simple formulae are sufficiently accurate that sophisticiated numerical modeling of temperatures in specific regions is unwarranted. Putain. An application of these simple formulae to measurements of conductive heat flow at island arcs implies that shear stresses at island arcs approach 100 MPa and are greater than 30 MPa. Calculations of temperatures appropriate for the Himalaya suggest that shear stresses of 100 MPa on the Main Central Thrust probably are required to account for the Tertiary granites of the region, if melting took place after slip began on the thrust. Similarly, the cut-off in seismicity at a depth of about 15 km in the Himalaya, if due to temperatures exceeding 350° to 450°C, implies a deviatoric stress close to 100 MPa.

INTRODUCTION

Despite accurate descriptions of the relative motions of lithospheric plates, of the rates of deformation in well studied, tectonically active regions, and of the strain fields in exhumed orogenic belts, the magnitudes of the stresses responsible for tectonic deformation remain controversial [*Hanks and Raleigh*, 1980]. Some Earth scientists [e.g., *Brace and Kohlstedt*, 1980; *Christie and Ord*, 1980; *Hanks*, 1977; *Oxburgh and Turcotte*, 1970; *Scholz*, 1980, *Scholz et al.*, 1979; *Toksöz et al.*, 1971; *Turcotte and Schubert*, 1973] have suggested that shear stresses in excess of 100 MPa (1 kbar) must drive the deformation manifested by earthquakes and mountain building. Others [e.g., *Brune et al.*, 1969; *Dalmayrac and Molnar*, 1981; *Lachenbruch and Sass*, 1973, 1980; *McKenzie and Jarvis*, 1980; *Mount and Suppe*, 1987; *Tapponnier and Molnar*, 1976; *Zoback et al.*, 1987] have argued that mean stresses on major faults are distinctly smaller than 30 MPa. This controversy also pervades discussions of the heat sources responsible for metamorphism and anatexis, because dissipation on rapidly slipping faults has been considered by some [e.g., *Barton and England*, 1979; *Graham and England*, 1976; *Scholz, et al.*, 1979; *Sibson*, 1980], but not all [e.g., *Bird*, 1978; *Molnar et al.*, 1983], to be an important source of heat.

Two questions, interconnected by the importance of shear heating, motivated the present study. The more general question is: What is the value of shear stress on the major thrust faults, such as at subduction zones? Just as heat flow measurements near the San Andreas fault have been used to place a constraint on the average stress on that fault [*Brune et al.*, 1969; *Henyey and Wasserburg*, 1971; *Lachenbruch and Sass*, 1973, 1980], we hope to do the same for subduction zones, for the moment using existing heat flow measurements, but eventually with more comprehensive measurement programs. The second, more parochial, question is: What are the heat sources responsible for anatexis, and perhaps also metamorphism, near the Main Central Thrust in the Himalaya?

[1]Permanently at Department of Earth, Atmosphere and Planetary Sciences, Massachusetts Institute of Technology, Cambridge.

Paper number 89JB03089.
0148-0227/89/89JB-03089$05.00

Shear Stress at Subduction Zones.

The energy radiated as seismic waves by earthquakes depends only upon the change in stress on the causative faults, and not on the magnitude of stress [e.g., *Brune and Allen*, 1967]. Because stress drops associated with earthquakes rarely exceed 10 MPa [e.g., *Hanks*, 1977], if mean stresses on actively slipping faults are significantly larger than 10 MPa, a substantial amount of energy must be dissipated near them. The small surface energies of rock forming minerals [e.g., *Brace and Walsh*, 1962; *Olgaard and Brace*, 1983] imply that the fracturing of minerals and the creation of new surfaces do not expend much energy [e.g., *Lachenbruch and Sass*, 1980]. Thus, if stresses on faults are high, the energy dissipated by friction is likely to be released as heat.

This logic stimulated an effort to measure heat flow along the San Andreas fault in order to constrain the average shear stress on that fault [*Brune et al.*, 1969; *Henyey and Wasserburg*, 1971; *Lachenbruch and Sass*, 1973, 1980]. The neglible anomalous heat flux measured near the fault has been widely, but not unanimously, accepted as evidence that the mean stress must be less than 20–30 MPa. In contrast, *O'Neil and Hanks* [1980] suggested that hydrothermal convective transport of heat near the San Andreas fault is large and that measurements of conductive heat flux in California underestimate the total flux. They suggest that the shear stress is much larger than 30 MPa.

One might imagine that convective circulation above the hanging wall of major thrust faults, such as those at subduction zones, is less than that near a shallow, vertical strike-slip fault. Moreover, stresses in regions of thrust faulting should be larger than those along strike-slip faults, as measurements suggest they are [*McGarr*, 1980]. Finally, because rates of slip at subduction zones are three to four times that on the San Andreas fault, and because dissipative heat generation is proportional to the product of shear stress and slip rate, the flux of heat between the trench and the volcanic arc might provide a more definitive constraint on the magnitude of the stress on such major faults. Thus, an analysis for thrust regimes could yield bounds of stresses different from those for strike-slip faulting.

Heat Sources Responsible for Tertiary Melting in the Himalaya

Two simple geologic facts suggest a major influence of thrust faulting on the thermal evolution of the region surrounding the Main Central Thrust in the Himalaya, and of such regions in general.

First, the metamorphic grade near the Main Central Thrust is commonly inverted, increasing up section before decreasing again [e.g., *Gansser*, 1964; *Le Fort*, 1975; *Valdiya*, 1980]. Dissipative heating has been suggested by several authors as the cause of inverted thermal gradients near major fault zones [e.g., *Arita*, 1983; *Barton and England*, 1979; *Graham and England*, 1976; *Scholz* 1980]. Several other mechanisms could, however, have caused an inversion in metamorphic grade, including late, brittle thrust faulting of high grade rock from depth onto lower grade rock at the surface [e.g., *Brunel and Kienast*, 1986; *Hubbard*, 1989], or the intrusion of hot anatectic granitoids into the upper thrust plate [e.g., *Brunel and Kienast*, 1986; *Hodges et al.*, 1988].

Secondly, Late Cenozoic anatectic granitoids crop out widely in the hanging wall of the Main Central Thrust and surely represent melting of the crust whilst or shortly after slip on that fault was occurring [e.g., *Le Fort*, 1981, 1986, 1988]. The remarkable similarity of the ratios of oxygen isotopes in one formation in the hanging wall to those in the neighboring Manaslu granite [e.g., *France-Lanord et al.*, 1988, *Vidal et al.*, 1982] strongly implies that the granite was derived from the hanging wall. The deformation of the Chhokang arm of the Manaslu granite just above the Main Central Thrust [*Le Fort*, 1981] implies that melting was roughly synchronous with slip on that fault. Similarly, the most reliable date, of 18.1 Ma, of the Manaslu granite [*Deniel et al*, 1987], is close to *Hubbard and Harrison's* [1989] $^{40}Ar/^{39}Ar$ age of 20.9 ± 0.1 Ma of minerals that grew during deformation within the Main Central Thrust zone. Thus, the leucogranites seem to have formed while the Main Central Thrust was active. In the absence of shear heating, movement on the fault should have cooled the region where melting occurred. The prograde metamorphism might also have been accompanied by the development of an inverted thermal gradient. The melting and the inverted metamorphism have been interpreted in a wide variety of ways, but none of the interpretations rests on a quantitative treatment of the thermal development of major thrust zones.

Development of Thermal Profiles During Thrust Faulting

A principal obstacle to investigating the problems posed above has been the difficulty of treating fully the thermal development of the upper block as the temperature profile of the lower block is advected beneath it. Slip on a thrust fault can affect the temperature distribution in the overlying hanging wall in at least three ways. First, displacement of the relatively cool footwall, downward along the fault, should draw heat from the overlying hanging wall and cool it. Second, the gradual emplacement of initially shallow, and therefore radiogenic, crust beneath the hanging wall can eventually cause an increase in temperature. Third, shear heating along the fault will cause an increase in temperature near it. Whether the temperature in the hanging wall rises or falls, and the precise evolution of such changes depend upon several parameters: the magnitudes and distributions of the three sources of heat (conduction from below, radioactivity, and shear heating), the rate at which displacement of the lower block of the fault advectively removes heat, and the physical properties of the medium (particularly, its coefficients of thermal conductivity and thermal diffusivity).

Because of the large number of parameters that affect the thermal evolution of such a region, and the difficulties in identifying the influences of each, most studies have considered simplifications for the advective transport of heat. The principal simplifications have been to consider diffusion of heat only in the vertical direction and to simulate thrust faulting by an instantaneous juxtaposition of the hanging wall, with its initial steady state geotherm, over the footwall whose initial surface temperature is zero [e.g., *Bickle et al.*, 1975; *Brewer*, 1981; *England*, 1978; *England and Thompson*, 1984; *Molnar et al.*, 1983; *Oxburgh and Turcotte*, 1974]. Shear heating can be accommodated as a point source in such a one-dimensional configuration [*Turcotte and Schubert*, 1973].

To elucidate and to quantify the roles played by lateral heat conduction and by advection, we carried out a series of numerical experiments of the time-dependent temperature distribution within a two-dimensional region cut by a thrust fault and with different sources of heating. We begin with a brief discussion of the approach that we take to solve the heat flow equation in a region undergoing thrust faulting. Then we consider some simple theoretical arguments that allow us to predict that temperature field, and we compare the numerical experiments with these simple theoretical formulae. Finally, with theoretical formulae justified by experiment, we use them to analyze measurements of heat flow at subduction zones and estimates of temperature in the neighbourhood of the Main Central Thrust.

METHOD

We are concerned with the transfer of heat by two mechanisms: conduction and advection. Because the advective transfer is effected by the rigid-body translation of one block in contact with another, we need not include advection explicitly in the equations governing heat transfer. Instead we solved the diffusion equation in each block separately, and we included advection by displacing the blocks at each time step and matching the boundary conditions on their common interface, the fault (Appendix A).

The physical model consists of blocks extending infinitely in the horizontal direction parallel to the strike of the fault and in contact at a planar fault (Figure 1). The upper block is triangular in cross section, with the top equivalent to the Earth's surface, where the temperature is fixed to be zero. The lower block is rectangular in cross section. The area of interest to us is near where the fault reaches the surface. We chose dimensions such that the vertical boundary on the upper block, across which there is no heat flux, is far from the area of interest. We ignore flexure of the lower block, and consequently the top surface of the lower block in the part of the model where that surface represents the Earth's surface has the peculiarity of being inclined parallel to the fault. This geometry simplifies the mathematics without introducing an important error.

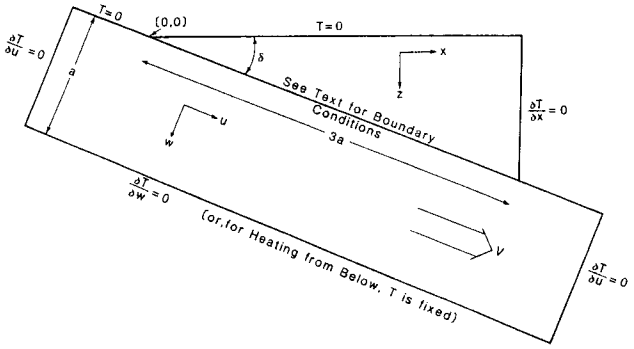

Fig. 1. Simple cross section of the two-dimensional model of a thrust fault and the blocks surrounding it. Coordinates systems and boundary conditions for the two blocks are shown.

The temperature distribution in the neighbourhood of a major thrust fault depends upon the relative amounts of heating due to three separate processes: (1) convective heat transfer to the base of the lithosphere and conduction of that heat through the lithosphere, (2) radioactive heating within the upper and lower blocks, and (3) shear heating due to slip on the fault. Because the heat flow equation is linear, we can consider the different heat sources separately, and by doing so, we

TABLE 1. Parameters Used in Derivations and Numerical Experiments

Parameter	Definition
T	temperature
t	elapsed time
(x, z)	coordinates (horizontal, vertical) in upper block
(u, w)	coordinates (parallel, perpendicular) to top of lower block, and to the thrust fault
(x_f, z_f)	coordinates in upper block of a point on fault
$(u_f, 0)$	coordinates in lower block of a point on fault
Q	heat flux at the Earth's surface
a	thickness of the lithosphere (the lower block)
κ	thermal diffusivity
K	coefficient of thermal conductivity
T_0	temperature at the base of the lithosphere $= Q_0 a/K$, for heating from below $= A_0 D^2/K$, for radiogenic heating $= \sigma V a/K$, for shear heating
Q_0	heat flux at the base of the lithosphere
δ	dip of thrust fault, $0° \leq \delta \leq 45°$
V	rate of slip (underthrusting) on the thrust fault
D	scaling depth for radiogenic heat production
A_0	radiogenic heat production, per unit volume per unit time, at Earth's surface
σ	shear stress on the thrust fault
μ	constant of proportionality between shear stress and depth on fault
t_1	$= u_f/V$ time for the footwall to slide a distance u_f under the upper block
t_2	$= z_f^2/(\pi^2 \kappa)$ thermal time constant for hanging wall where depth of fault is z_f

can understand at least some of the factors that affect the evolution of the temperature regime with time, as opposed simply to calculating the temperature field for a small subset of the geologically plausible scenarios.

Heat transport is governed by

$$\frac{\partial T}{\partial t} = \kappa \nabla^2 T - \mathbf{V}.\nabla T + \frac{A}{\rho c} \tag{1}$$

for which all parameters are defined in Table 1. For heating from below the plate and for shear heating, $A = 0$, but when radioactive heating is considered, we let $A(z) = A_0 \exp(-z/D)$. Note that oblique slip can be treated by using the component of velocity in the direction of the dip.

In all numerical experiments, we solved this equation in dimensionless form, with distances scaled by lithospheric thickness, a, and times by a^2/κ. The velocities were made dimensionless by dividing by the rate of slip on the faults, V. Temperatures were rendered dimensionless by $T' = T/T_0$, and each source of heating was also scaled to T_0, see Table 2. Thus, in dimensionless form, (1) becomes

$$\frac{\partial T'}{\partial t'} = \nabla'^2 T' - \mathrm{Pe}\mathbf{V}'.\nabla' T' + A' \tag{2}$$

where $\mathrm{Pe} = Va/\kappa$ is the Peclet number, and the other scalings are given in Table 2.

TABLE 2. Dimensionless Parameters Used in Numerical Experiments.

Parameter	Definition
(x', z', u', w')	$(x, z, u, w)/a$
(x'_f, z'_f, u'_f)	$(x_f, z_f, u_f)/a$
t'	$\kappa t/a^2$
T'	T/T_0
	$= TK/Q_0 a$, for heating from below
	$= TK/A_0 D^2$, for radiogenic heating
	$= TK/\sigma V a$, for shear heating
Pe	Va/κ, Peclet number
D'	D/a
A'	Aa^2/KT_0
σ'	$\sigma\kappa/KT_0$

For heating from below or for shear heating, the dimensionless temperature field depends on only two dimensionless quantities, the dip of the fault, δ, and Peclet number. For radioactive heating, there is a third dimensionless parameter, $D' = D/a$, the dimensionless depth scale of the distribution of radioactivity. Our procedure was to carry out numerical experiments by varying systematically δ and Pe (and D' for radioactive heating) and examining the dependence of the calculated temperature field on these quantities.

THEORY

We derive simple formulae for the initial changes in the temperature field along the fault with time and for the steady state temperature distribution in the upper block. Let us consider them separately and for each, let us consider separately the three sources of heat — heating from below the lithosphere, radioactive heating within the blocks, and shear heating along their common interface.

Changes in Temperature Along the Fault at Short Times

For heating only from below, the initial temperature distribution is given by

$$\begin{aligned} T(x, z) &= Q_0 z/K \\ T'(x', z') &= z' \end{aligned} \tag{3}$$

If the Peclet number is sufficiently large, we can ignore conduction and examine the change in temperature due only to the movement of cold material below the fault and its juxtaposition to the warmer overlying block. The temperature at a point on the fault at time $t + \Delta t$ should be the average of the temperature at that point at time t and the temperature at $u - \Delta u$ also at time t, where $\Delta u = V\Delta t$ (Figure 1). Thus at any point along the fault,

$$T(u, 0, t + \Delta t) = \frac{1}{2}\left[T(u, 0, t) + T(u - \Delta u, 0, t)\right] \tag{4}$$

The temperature at $u - \Delta u$ is approximately

$$T(u - \Delta u, 0, t) = T(u, 0, t) - \Delta u \frac{\partial T}{\partial u} \tag{5}$$

Combining terms, we have

$$T(u, 0, t + \Delta t) - T(u, 0, t) = -\frac{1}{2} V \Delta t \frac{\partial T}{\partial u} \tag{6}$$

In the limit of vanishing Δt, and with $\partial T/\partial u = \partial T/\partial z \sin\delta$ we have

$$\frac{\partial T}{\partial t} = -\frac{1}{2} V \frac{\partial T}{\partial z} \sin\delta \tag{7}$$

Because $\partial T/\partial z = Q_0/K$

$$\begin{aligned} \frac{\partial T}{\partial t} &= -\frac{1}{2}\frac{Q_0 V \sin\delta}{K} \\ \frac{\partial T'}{\partial t'} &= -\frac{1}{2}\mathrm{Pe}\sin\delta \end{aligned} \tag{8}$$

Hence for points on the fault [(x_f, z_f), where the subscript f denotes a point on the fault (Table 1)] in the early stages of slip:

$$\begin{aligned} T(x_f, z_f, t) &= \frac{Q_0(z_f - \frac{1}{2}Vt\sin\delta)}{K} \\ T'(z'_f, x'_f, t') &= z'_f - \frac{1}{2}\mathrm{Pe}\ t'\sin\delta \end{aligned} \tag{9}$$

Deviations from this linear change with time must occur when $t \simeq z_f/(V\sin\delta)$, or $t' \simeq z'_f/(\mathrm{Pe}\sin\delta)$, for at that time the (Earth's) surface, initially with both $T = 0$ and $\partial T/\partial u = 0$, will have reached the point in question.

For radioactive heating, we can use the same development, but the temperature gradient, $\partial T/\partial z$, inserted into (7) varies with depth:

$$\frac{\partial T}{\partial z} = \frac{A_0 D}{K}\left[e^{-z/D} - e^{-a/D}\right] \qquad (10)$$

Consequently, the temperature on the fault should vary with time as slip occurs on the fault. The initial rate should be most rapid at shallow depths and decreases to nil at depths $z_f \gg D$, but at shallow depths the rate can increase with time before decreasing.

For shear heating, the initial warming of both the upper and lower blocks should be similar to that resulting from the instantaneous application of a heat source to the surface of a half-space. Half of the heat production, per unit area per unit time, will warm the upper block and half the lower one. Using *Carslaw and Jaeger's* [1959, p. 75] formula for temperature as a function of time and distance y from the surface of such an equivalent half-space, with a heat source of $\sigma V/2$, we have

$$T(y,t) = \frac{\sigma V}{K}\left[\sqrt{\frac{\kappa t}{\pi}}e^{-y^2/4\kappa t} - \frac{y}{2}\mathrm{erfc}\left(\frac{y}{2\sqrt{\kappa t}}\right)\right] \qquad (11)$$

where y is distance from the plane of heating. The temperature at the interface (corresponding to $y = 0$) should be

$$\begin{aligned} T(t) &= \frac{\sigma V}{K}\sqrt{\kappa t/\pi} \\ T'(t') &= \sigma' \mathrm{Pe}\sqrt{t'/\pi} \end{aligned} \qquad (12)$$

When the rate of heating is independent of depth, rocks on either side of the fault have the same history of heating, and the temperature distribution is symmetrical about the fault until either the boundary condition at the top of the top block affects the temperature at depth or until the area originally at the surface reaches the position under consideration. The approximate expressions should, therefore generally apply until the smaller of $t \simeq z_f^2/\pi^2\kappa$ or $t \simeq u_f/V$). When the rate of heating increases with distance down the fault (for instance owing to a constant coefficient of friction) the rocks in the upper block experience a greater rate of heating than do the rocks in the lower block directly beneath them. Consequently, the temperatures are not symmetrical about the fault and the one-dimensional expressions become inappropriate at shorter times.

Steady State Temperature Distribution in the Upper Block

In steady state, the temperature field in the upper block does not change with time, and as the lower block slides beneath the upper one, its top surface comes in contact with an increasingly hotter bottom of the upper block. The lower block block warms, but in steady state, seen in a coordinate system fixed to the upper block, the temperature field below the fault does not change (Figure 2).

If lateral conduction of heat parallel to the fault along the lower block is slow compared with conduction into the block from the fault and perpendicular to it, then the temperature in the lower block at any time is analogous to that in a semi-infinite, one-dimensional medium, at whose surface the temperature increases with time. The precise form of the increase along the fault of the steady state temperature remains to be determined, but we can consider a wide range of possible conditions by using solutions for temperatures in a one-dimensional medium whose surface temperature increases with time as: $T(0,t) = \alpha t^{m/2}$, with m an integer (Appendix B). The temperature gradient at the surface of the medium is given by

$$\frac{\partial T}{\partial y} = -b\frac{T(0,t)}{\sqrt{\kappa t}} \qquad (13)$$

where y is distance from the surface; b depends weakly on m and is defined by (B5). We may use this result to estimate the steady state temperature T at a distance u_f along the fault. The plane $y = 0$ in (13) corresponds to the fault surface at u_f, and the time taken for a rock at the top of the lower block to travel a distance u_f along the fault is given by $t = u_f/V = x_f/(V\sin\delta)$ (see Figures 1 and 2). Hence the boundary condition $T(0, t = u_f/V) = \alpha t^{m/2}$ discussed in Appendix B, is

TEMPERATURES IN THE LOWER BLOCK SLIDING BENEATH THE UPPER BLOCK AT STEADY STATE

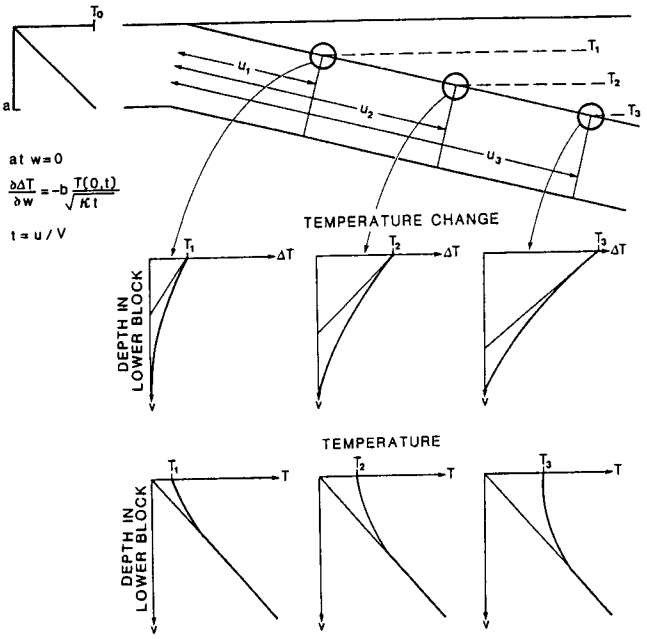

Fig. 2. Plots of changes in temperature and temperature profiles in the lower block as it slides beneath the upper block. Initially the temperature in the lower block increases linearly with depth (insert in upper left). As the lower block slides beneath the upper one the temperature at $w = 0$ on the upper surface of the lower block increases linearly with time. Notice that while the temperature change $\Delta T(0,t)$ is initially zero and increases linearly with time, the gradient in ΔT at the surface decreases more slowly: $\partial \Delta T/\partial w|_0 = -b\Delta T(0,t)/\sqrt{\kappa t}$. See Appendix B for more details.

analogous with the temperature along the fault: $T_f(u = u_f, w = 0)$ in the lower block, or $T_f(x_f, z_f)$ in the upper block.

The gradient given by (13) represents the diminution in heat flux across the upper surface of the lower block that results from its contact with the warm overriding block for the interval of time, t. The factor b depends upon the way in which the temperature at the surface of the one-dimensional medium changes with time – or in which the temperature at the top surface of the lower block varies with distance down the fault. If the temperature increased proportionally to the square root of time (that is if $m = 1$), the value of b would be $\sqrt{\pi/2} \simeq 0.886$ (B5); and it would be $2/\sqrt{\pi} \simeq 1.128$, if the temperature increased linearly with time ($m = 2$). The results of the numerical experiments (discussed below) demonstrate that the assumption that b is approximately equal to one is a useful one.

Conduction of heat from below. At depth z_f on the fault the temperature is initially $Q_0 z_f/K$. Let $T_f(z_f)$ be the, as yet unknown, steady state temperature at that point (Figure 3*a*). There are no heat sources within either block, so the steady state vertical temperature gradient at the fault must be approximately equal to T_f/z_f. There are no heat sources at the fault, so the heat flux on either side of the fault must be KT_f/z_f. The top of the lower block will have warmed as it slid beneath the upper block, and the initial flux Q_0 through it will have diminished. From the arguments given above, that decrease in the flux should be given by $bKT_f/\sqrt{\kappa t} = bKT_f/\sqrt{\kappa u_f/V}$. Equating the flux out of the lower block to that through the upper block yields

$$KT_f/z_f = Q_0 - bKT_f/\sqrt{\kappa u_f/V} \qquad (14)$$

We neglect the different orientations of the upper and lower blocks, which manifests itself as a factor of $\cos\delta \simeq 1$. Rearranging, using $z_f = u_f \sin\delta$, we have

$$T_f = \frac{Q_0 z_f/K}{1 + b\sin\delta\sqrt{u_f V/\kappa}} \qquad (15)$$

Notice that the temperatures given by (15) can be recognized as the steady state temperatures that would

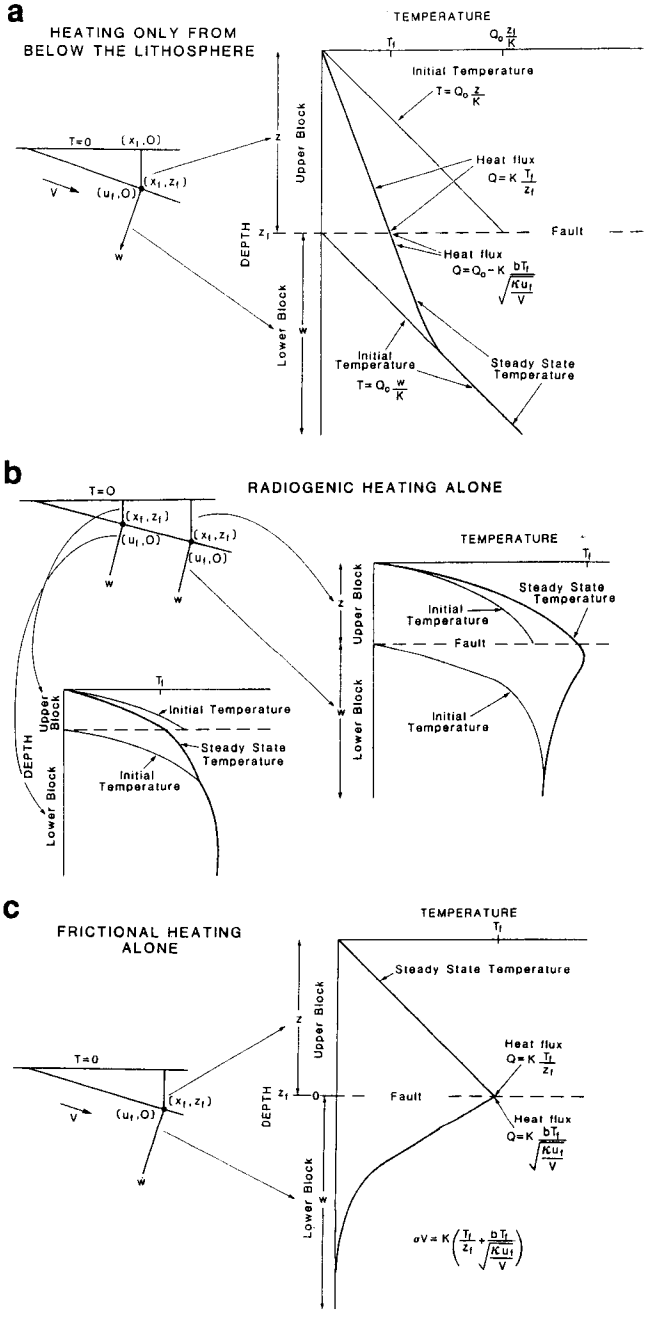

Fig. 3. Plots showing the forms of initial and steady state temperature profiles in the upper and lower blocks for the three types of heating: (*a*) heating from below, (*b*) radiogenic heating, and (*c*) shear heating on the fault plane. In (*a*), the temperature in each block initially is linear. When steady state is reached, the temperature at the fault is lower, but the gradient in the upper block is uniform. The upper part of the lower block is warmed, as it slides beneath the upper block, but the gradient deep in the lower block is unchanged. By analogy with the case in Appendix B and Figure 2, the flux of heat from the upper part of the lower block into the upper block is reduced from Q_0 by the term: $KbT_f/\sqrt{\kappa t}$, where $t = u_f/V$ is the time for the surface of the Earth to reach the point in question. Similarly, in (*b*), initial and steady state temperature profiles are shown for the case where heating is entirely internal and decreases exponentially with original depth in each block. For shallow depths along the fault (lower left), the cold lower block has drawn heat from the warmer upper one, and steady state temperatures are lower than the initial values. For sufficiently great depths, however, the advection of material with radiogenic heat producing elements near the surface of the lower block causes the temperatures along the fault and in the upper block to be larger than their initial values. In (*c*), heat generation due to dissipation on the fault causes heat to flow into the upper and lower blocks. Initially, $T = 0$ throughout the region. At steady state, the flux of heat into the upper block is given simply by KT_f/z_f, and that into the lower block is approximately given by $KbT_f/\sqrt{\kappa t}$, where once again $t = u_f/V$. The total flux of heat must equal that produced on the fault: σV.

exist in the absence of advection (in this case equal to the initial temperatures $Q_0 z_f/K$) reduced by the divisor

$$\begin{aligned} S &= 1 + b \sin\delta \sqrt{u_f V/\kappa} \\ &= 1 + b\sqrt{z_f V \sin\delta/\kappa} \\ &= 1 + b\sqrt{\mathrm{Pe} z_f' \sin\delta} \end{aligned} \tag{16}$$

We can use the form of (15) to estimate b. When z_f' and Pe are small, $S \simeq 1$, and $T_f' = z_f'$. In the analogy with the one-dimensional medium, $m = 2$, and using (B5), $b = 2/\sqrt{\pi} = 1.128$. When z_f' or Pe is large, $S \propto \sqrt{z_f'}$, and $T_f' \propto z_f'^{\frac{1}{2}}$. In the same analogy, $m = 1$, and $b = \sqrt{\pi}/2 = 0.886$. We use the numerical results to determine the factor b, but from these arguments, we should expect that over a broad range of z', on the average $b \simeq 1$.

Radioactive heating. We derive a similar result to that above by using similar arguments (Figure 3*b*). At steady state, the temperature in the upper block is given by

$$T = \frac{A_0 D^2}{K}\left[1 - e^{-z/D}\right] - \frac{A_0 D z}{K} e^{-z_f/D} + \frac{Q_f z}{K} \tag{17}$$

where Q_f is the total heat conducted from the lower block across the fault into the upper block. Q_f is diminished below its steady state value (which is $A_0 D[1 - e^{-a/D}] \simeq A_0 D$) owing to contact with the upper plate. Again, the amount by which the heat flux is diminished may be approximated by $-bKT_f/\sqrt{\kappa t}$, where T_f is the temperature on the fault at $z = z_f, t = u_f/V$. Combining these terms gives

$$Q_f = A_0 D\left[1 - e^{-a/D}\right] - \frac{bKT_f}{\sqrt{\kappa u_f/V}} \tag{18}$$

which clearly can be positive or negative. Substituting (18) into (17) yields

$$T_f = \left[\frac{A_0 D^2}{K}\left[1 - e^{-z_f/D}\right]\left[1 + \frac{z_f}{D}\right] - \frac{A_0 D z_f}{K} e^{-a/D}\right]/S \tag{19}$$

Note that the numerator gives the temperature on the fault that would exist in the absence of advection, and that the same divisor S, present in the case for heating only from below and given by (16), reduces that temperature.

Notice that for $z_f \ll D$, and such that $S \simeq 1$, $T_f \simeq A_0 D z_f/K$, corresponding to $m = 2$ in Appendix B, and we might expect $b = 2/\sqrt{\pi}$. For $z_f \gg D$, $T_f \simeq A_0 D z_f/KS$, and $S \propto z_f^{\frac{1}{2}}$, so that $T \propto z_f^{\frac{1}{2}}$ corresponding to $m = 1$, and $b = \sqrt{\pi}/2$.

Shear heating. The rate of heat generation (per unit area per unit time) on the fault is given by the product of the shear stress and the rate of slip: σV. Some of the heat will be conducted upward and some will warm the lower plate. When steady state is reached, the fraction conducted upward will be defined by the steady state temperature on the fault, $T_f(z_f)$, and the heat flux in the vertical direction should be KT_f/z_f, once again assuming that lateral conduction of heat is negligible. The flux perpendicular to the fault into the lower block will be given approximately by $-bKT_f/\sqrt{\kappa u_f/V}$ (Figure 3*c*). The difference in heat flux across the fault must be σV:

$$KT_f[1/z_f + b/\sqrt{\kappa u_f/V}] = \sigma V \tag{20}$$

and

$$T_f = \frac{\sigma V z_f/K}{S} \tag{21}$$

Let us consider two possible forms of shear heating. In one, let the stress, σ, be constant, and in the other, let it be proportional to the depth: $\sigma = \mu z_f$, as would be the case, for example, in sliding with a constant coefficient of friction. In the absence of advection, and with no flux at the base of the lower block, the steady state temperature at a depth z_f due to a localized shear heating of σV would be $\sigma V z_f/K$. For a localized heat source at the depth z_f due to shear heating at a rate proportional to depth, the steady-state temperature would be $V\mu z_f^2/K$, and (21) becomes

$$T_f = \frac{V\mu z_f^2/K}{S} \tag{22}$$

In either case, the influence of advection is to reduce the steady state temperature by a divisor given by (16), but note that the temperature profile along the fault for one case (21) varies as z_f/S and for the other (22) it varies as z_f^2/S. From the analogy described in Appendix B, the factor b should be different in the two cases. For constant stress, as for heating from below, $b \simeq 1$. For stress proportional to depth, however, $T_f \simeq z_f^2$ for small z_f or small Pe, and $T_f \simeq z_f^{3/2}$ for large values of them. Hence, from the analogy in Appendix B, we might expect $b \simeq 8/3\sqrt{\pi} \simeq 1.5$ for small z_f and Pe and $b \simeq 3\sqrt{\pi}/4 \simeq 1.3$, for large values of them.

Summary. Equations (15), (19), (21), and (22) yield expressions for the temperature at a given depth or distance along the fault. These are based on the assumption that lateral heat conduction can be neglected, and therefore together with the distribution of radioactivity in the upper block they uniquely define the temperature field within that block. In the absence of internal heat sources, such as that due to radioactivity, the gradient in the upper block should be constant. Thus, for example, for heating from below and shear heating at constant stress, the steady state temperature should be given by

$$T(z) = \frac{(Q_0 + \sigma V)z/K}{S} \tag{23}$$

For radiogenic heating, there can be heat flux from the lower block into the upper one, but at shallow enough depths or high enough Peclet number, heat pro-

duced in the upper block may flow downward across the fault into the lower block. The temperature field in the upper block due to all three sources of heating is given by

$$T(z) = \frac{A_0 D^2}{K}\left[1 - e^{-z/D}\right] - \frac{A_0 D z}{K} e^{-z_f/D} + \frac{(Q_0 + \sigma V)z/K}{S} + \frac{Q_f z}{K} \quad (24)$$

The first two terms give the contribution to temperature from radioactivity in the upper block. The third and fourth terms represent the flux into the base of the upper block; this flux is equal to the steady-state flux into the base of the upper block in the absence of movement, but divided by the factor S in (16). The last of these terms, $Q_f z/K$, contains S implicitly, as defined by (15) and (19), and can be negative. Thus the steady-state temperature field in the upper block can be given in closed form. Other distributed or local heat sources, for instance associated with metamorphic reactions or penetrative shear heating, can be included in the same fashion.

Time Constants for Steady State

There are two obvious characteristic times after which the temperature field should begin to approach steady state. One is the time needed for the region initially at the Earth's surface, where the initial temperature is zero, to reach the particular point on the fault:

$$\begin{aligned} t_1 &= u_f/V \\ &= z_f/V \sin\delta \\ t_1' &= u_f'/\mathrm{Pe} \\ &= z_f'/\mathrm{Pe}\sin\delta \end{aligned} \quad (25)$$

For distances of $u_f = 100$ km and and slip rates of $V = 100$, 10, or 1 mm/yr, t_1 is 1, 10, or 100 m.y. The other time constant is governed by the time needed to warm or cool an infinite slab of thickness z_f with one surface held at a constant temperature and that on the other changed instantaneously:

$$\begin{aligned} t_2 &= z_f^2/(\pi^2\kappa) \\ t_2' &= z'^2/\pi^2 \end{aligned} \quad (26)$$

For $z_f = 25$ or 50 km, $t_2 = 2$ or 8 m.y. The numerical experiments show that when times exceed the sum of these two time constants, the temperature field is close to steady state.

RESULTS OF THE NUMERICAL EXPERIMENTS

We carried out a series of experiments with $\delta = 5°$, 15°, 25°, and 45°, and for Pe = 3.16, 10.0, 31.6, 100, and 316 for all four sources of heat described above: heating from below, radiogenic heating, heating on the fault at a constant rate, and heating on the fault at a rate proportional to depth. For radioactive heating, we considered two values of D': 0.10 and 0.20. The essence of the theoretical development of the previous section is that lateral conduction of heat can be ignored and that the thermal evolution of the block overlying the fault is governed entirely by the change in temperature at the fault surface. Thus, most of the results that we show are either calculated temperatures at a few points along the fault as a function of time (Figures 4–6) or calculated steady state temperatures as a function of depth along the fault (Figures 7–10). These are compared with theoretically estimated values, and the resulting agreement offers support for the assumptions used to derive the theoretical relations.

Temperatures at Short Times.

The calculated temperatures for heating from below initially decrease according to (9). The agreement is best for large Peclet numbers, for which conduction does not affect the temperature field as much as advection does. For instance for $\delta = 5°$ or 25°, Pe = 316, the experimental data fit (9) for the entire duration of $t_1 = u'/\mathrm{Pe}$ (Figures 4*a* and 4*c*). For all Peclet numbers, however, eventually the rate of decrease in temperature diminishes, as steady state is approached, and for smaller Peclet numbers, this deviation from (9) begins before t_1 has elapsed (e.g., Figure 4*b*).

For shear heating, (12) describes the initial increase in calculated temperatures, with more success for constant stress (Figure 5*a*) than for heating at a rate proportional to depth (Figure 5*b*). When stress increases along the fault, movement on the fault juxtaposes rocks with different histories of heating, making the assumption of only one relevant dimension, implicit in the application of (12), less appropriate for depth-dependent stress than for a constant stress.

For radiogenic heating, the initial decrease in temperature obeys (7) and (10). At depths notably larger than D, the initial gradient is small, and even for large Peclet numbers, the initial rate of change with time is correspondingly small (Figure 6), as predicted by (7) and (10). At shallower depths, the initial rate of change with time is larger, as it should be where the initial gradient is relatively large (Figure 6). For some Peclet numbers, the rapid movement of cold material from near the surface to greater depths, where the initial gradient is very small, can cause the rate of decrease in the temperature along the fault to increase with time, before it decreases as steady state is approached (Figure 6*a*).

For heating from below the final temperatures are lower than those initially and for shear heating temperatures increase; for radiogenic heating final temperatures can be either greater or less than the initial values (Figure 6). For sufficiently large depths, the final temperatures will exceed the initial values, but the particular depth at which the initial and final temperatures are the same depends on the three relevant dimensionless parameters, and therefore on the dip, slip rate, and D. This is clear from the difference between the initial and theoretical steady state temperature distributions,

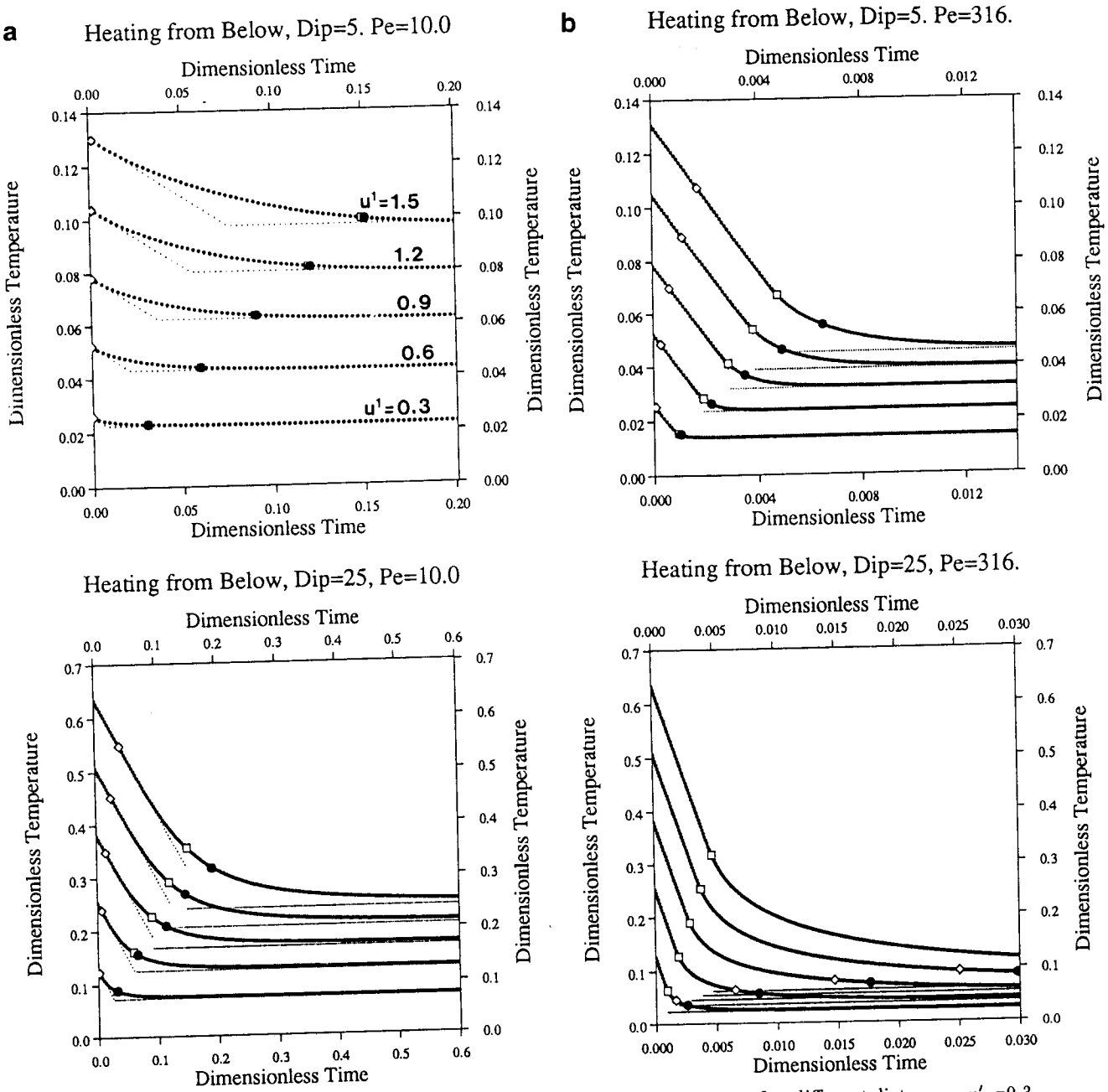

Fig. 4. Plots of dimensionless temperatures against dimensionless time at five different distances, $u' = 0.3$, 0.6, 0.9, 1.2, and 1.5, along a fault, dipping at $\delta = 5°$ and 25°, for heating from below and for two Peclet numbers: (*a*) Pe = 10.0, and (*b*) Pe = 316. The lowest curve is for the smallest distance, $u' = 0.3$. Large dots show results of numerical experiments sampled at every n dimensionless time steps (see Appendix A), and therefore at each time when grid points in the upper and lower blocks are aligned. Smaller dots defining finer lines show theoretical curves given by (10) for short times, and the steady state temperatures given by (15) for later times. Open diamonds and squares show the temperatures at t_1 and t_2 respectively. The solid circles show the temperatures at $(t_1 + t_2)$. Note that when $t \geq (t_1 + t_2)$ the temperature is nearly in steady state. Note also that for a large Peclet number, the rate of change is linear for essentially the entire duration of t_1. For the smaller Peclet number, deviations from this linear decrease occur at smaller fractions of t_1, because at a slower rate of underthrusting, $t_2 < t_1$, and the fixed temperature at the top surface influences the temperature history along the fault.

equations (A1) and (19). Let us neglect the term with the small factor $e^{-a/D}$ in each equation and compare the temperatures given by these two expressions. After a few lines of algebra, we obtain the condition that for the final temperature on the fault to exceed its initial value,

$$\begin{aligned} z_f &> D^2 V \sin\delta/\kappa \\ u_f &> D^2 V/\kappa \\ z'_f &> D'^2 \mathrm{Pe} \sin\delta \\ u'_f &> D'^2 \mathrm{Pe} \end{aligned} \qquad (27)$$

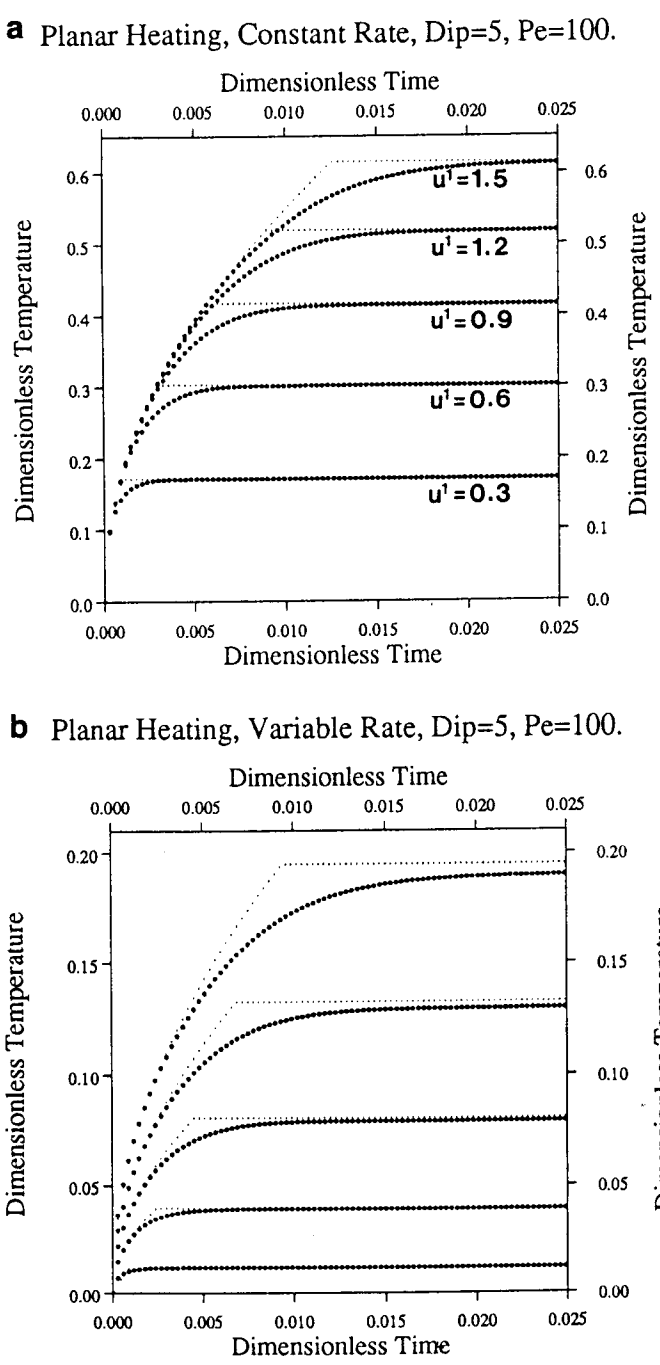

Fig. 5. Plots of dimensionless temperatures against dimensionless time at five different distances, $u' = 0.3$, 0.6, 0.9, 1.2, and 1.5, along the fault, for shear heating heating on the fault, (a) at a constant rate (σ' Pe = 9.723), and (b) at a rate increasing in proportion to the depth on the fault (μPe = 27.22). Symbols and layout as in Figure 4. For heating at a constant rate (a), the initial change in temperature follows very closely that given by (12) for nearly the entire duration of t_1. For a rate of heating increasing with distance along of the fault (b), deviations from (12) begin earlier.

For the largest values of Pe (100 or 316) and for $D' = 0.20$, the calculated dimensionless distances along the fault where initial and final temperatures should be the same are $u' = 4.0$ and 13, which are notably greater than the largest value of u'_f (= 1.5) considered here. However, for small Peclet numbers (10 or 31.6), and for the range of dimensionless distances along the fault shown ($u' = 0.3$ to 1.5 in Figure 6), the final temperatures exceed the initial ones for the larger but not smaller depths. For Pe = 31.6 and $D' = 0.10$, initial and steady state temperatures should be equal for $u' = 0.3$, as they are (Figure 6c). For $D' = 0.20$, however, steady state temperatures should exceed initial ones only for $u' = 1.3$, also approximately as observed (Figure 6d).

Steady State Temperatures.

For heating from below, advection causes a reduction in the steady state temperature and that reduction is greatest for the largest Peclet numbers and the greatest dips. The theoretical argument of the previous section suggests that all steady state temperatures along the fault are equal to those that would exist at the particular depth of the fault in the absence of advective heat transport, but divided by quantity S in (16). For heating from within and from below the lithosphere, and for heating at a constant rate on the fault, the theoretically predicted steady state temperatures on the fault, given by (15), (19) and (21), differ from those calculated in the numerical experiments by less than 5%, when the factor $b = 1.0$ in (16) (Figures 7, 8 and 9). Adjusting the value of b slightly (usually in the range 0.9–1.1: Table 3) produces theoretical curves that agree to better than 1% with the calculated temperatures. For shear heating at a rate proportional to depth, the theory outlined above predicts a value of b closer to 1.33 than to 1.0, and for most Peclet numbers, values of b in the range 1.27 and 1.35 yield differences between theoretical and calculated temperatures that are smaller than a few per cent of the calculated values (Figure 10, Table 3). For this mode of heating, using $b = 1$ yields roughly 30% differences between calculated and theoretical temperatures. The theory does not fit well for either value of b in the case with Pe = 3.16, for which the importance of lateral heat conduction is probably greatest (Figure 10). (Note that for shear heating, the heat sources were chosen to be the same for all values of Pe, by making the product σ Pe = const, or μ Pe = const.)

The agreement between the experimentally determined temperatures along the fault and those given by (15), (19), (21), and (22), constitutes a strong justification of the theoretical argument given in deriving (15)–(22). To emphasize that this argument allows the temperature field to be given throughout the upper block we show in Figure 11 the agreement between the experimentally determined temperatures along profiles through the upper block and those given theoretically by (24).

Times to Reach Steady State.

As noted above, two characteristic times are inherent in the physical processes controlling the temperature history. One is given by the interval of time for

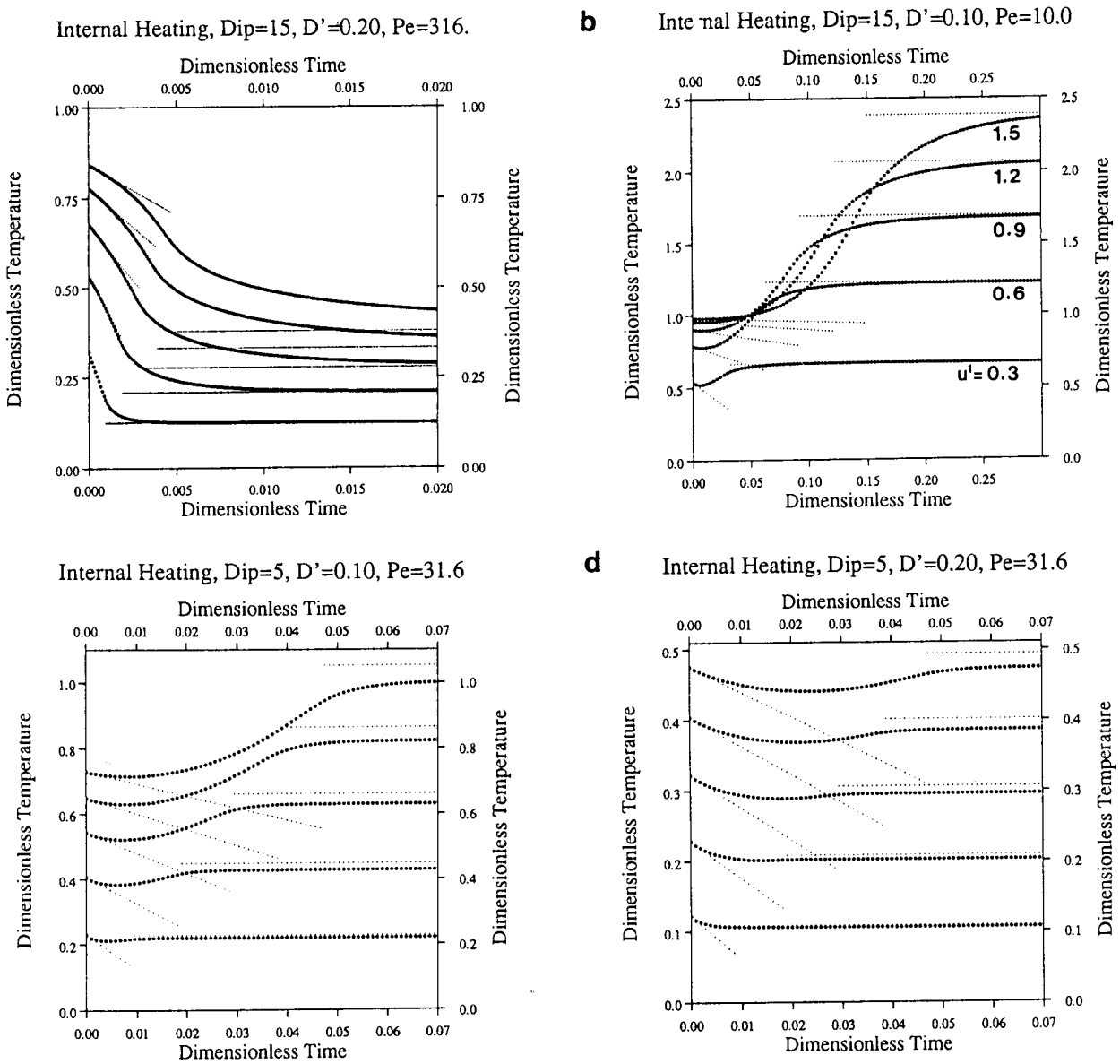

Fig. 6. Plots of dimensionless temperatures against dimensionless time at five different distances, u' =0.3, 0.6, 0.9, 1.2, and 1.5, along the fault, for internal heating. Symbols and layout as in Figure 8. For a large Peclet numbers, Pe = 316 (a), the final temperatures are lower than the initial values, but for small Peclet numbers, such as in (b), the opposite holds. For both the initial change in temperature is greatest at shallow depths, where the gradient initially is largest, but for a large Peclet number (a), the rate of decrease in temperature increases with time as increasingly colder material is thrust under the deeper part of the lower block. Whether the steady state temperature is larger or smaller than the intitial temperature depends upon both the Peclet number and D' according to (28). For Pe = 31.6, steady state temperatures should exceed intitial temperatures for $u' > 0.3$ for $D' = 0.10$, as observed in (c), but only for $u' > 1.3$ for $D' = 0.20$, as shown in (d). Note that for such combinations of Pe and D', the temperature can decrease initially but then exceed its initial value. In all cases, the dimensionless temperature at the base of the lower block has been set equal to unity by choosing the dimensionless heat generation at the surface, A_0', such that $A_0' D' = 1$.

the Earth's surface to reach the depth at the particular point on the fault in question, t_1, and the other is the thermal time constant for heating (or cooling) a slab with a thickness given by the depth of the fault, t_2 (Table 1). For rapid slip to a relatively large depth, t_1 is the shorter, but for shallow depths of the fault and low slip rates, t_2 is the shorter. For large Pe and depths for which t_2 is larger than t_1, the formulae for the initial changes in temperature, (9), (10), and (12), are accurate for elapsed times that are large fractions of t_1 (e.g., Figures 4a and 4c). When t_2 is comparable with or smaller than t_1, however, diffusion of heat into the whole of the upper block causes the initial change in temperature to apply only for a fraction t_1 (e.g., Fig-

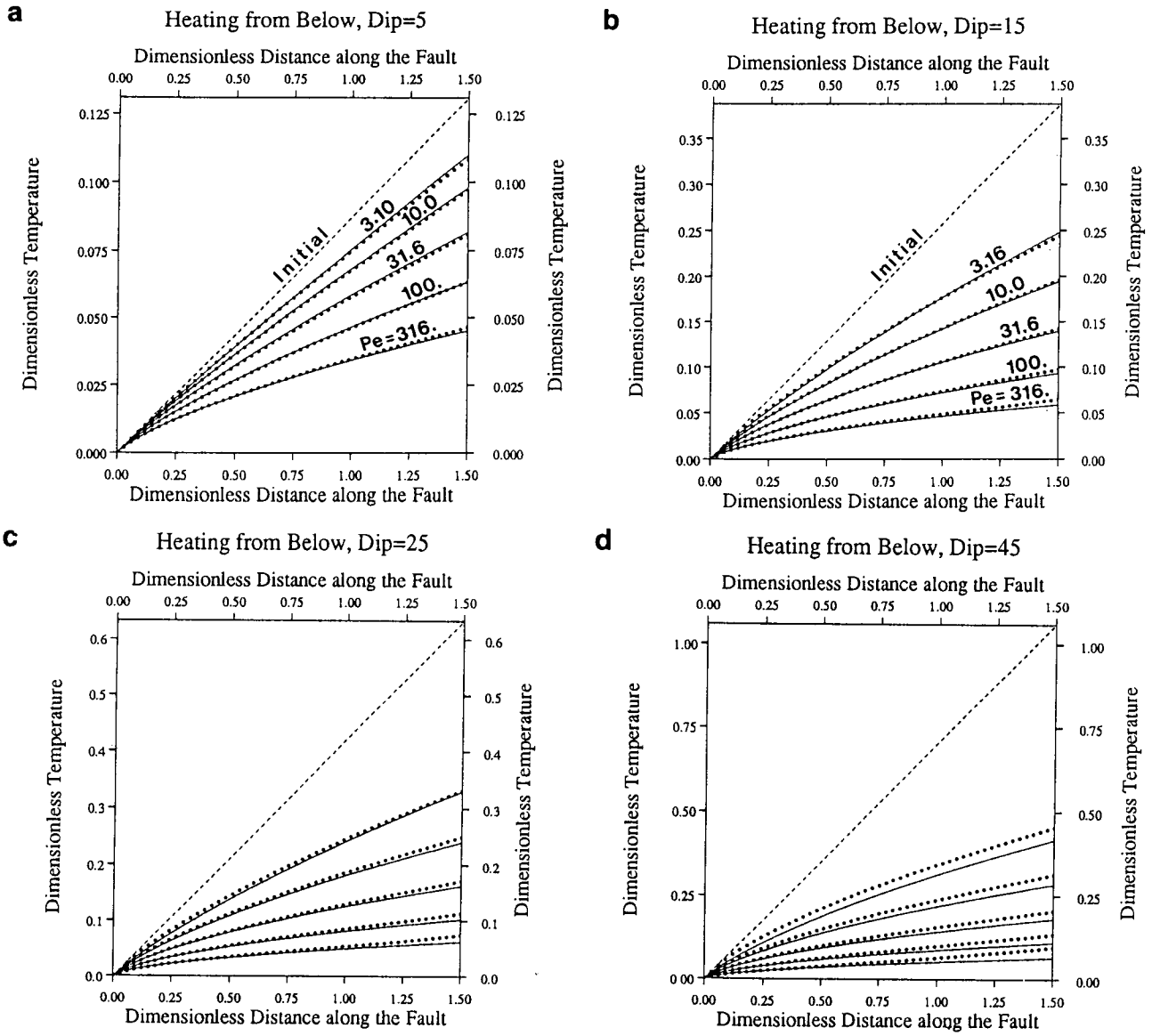

Fig. 7. Plots of dimensionless temperatures against dimensionless distances along the fault for heating from below. Each plot shows the initial temperature (dashed line) for a specific dip and results for several Peclet numbers. Solid symbols indicate results of numerical experiments, which were calculated at 50 intervals of $\Delta u'$. Continuous lines are defined by (15), with $b = 1$. Note that the change in temperature is greatest for large Peclet numbers, large dips, and large depths. Note also that the theoretical curves and experimental data differ by less than 5% in nearly all cases.

ure 4*b*). Thus the times given by both t_1 and t_2 mark deviations from the simple initial change in temperature given by (9), and in none of the experiments was steady state reached until the elapsed time exceeded substantial fractions of both t_1 and t_2.

For most experiments, when elapsed times exceed $(t_1 + t_2)$, the changes in calculated temperatures deviate by roughly 5%, and nearly always by less than 10%, from their ultimate changes or values. When the time exceeds $2(t_1 + t_2)$, nearly all deviate by less than 5% from their steady state values, and more than half deviate by less than 1%. The exceptions are at low Peclet numbers for heating from below, for which changes in temperature are small, and at large Peclet numbers for radiogenic heating.

Summary of the Results of the Numerical Experiments.

The numerical experiments confirm the applicability of the formulae given in (15), (19), (21), and (22) to predict the steady state temperatures on the fault, and they yield estimates of the factor b in (16) that allow the theoretical temperatures to match those calculated within one percent. The formulae in (9), (10), and (12) yield accurate estimates of the initial change in temperature with time. Deviations from those initial rates of change are noticeable after an elapsed time roughly equal to t_2 or to t_1, whichever is shorter, except for the case of shear heating at a rate proportional to depth, for which deviations begin sooner. Because steady state is approached when the time exceeds that given by the

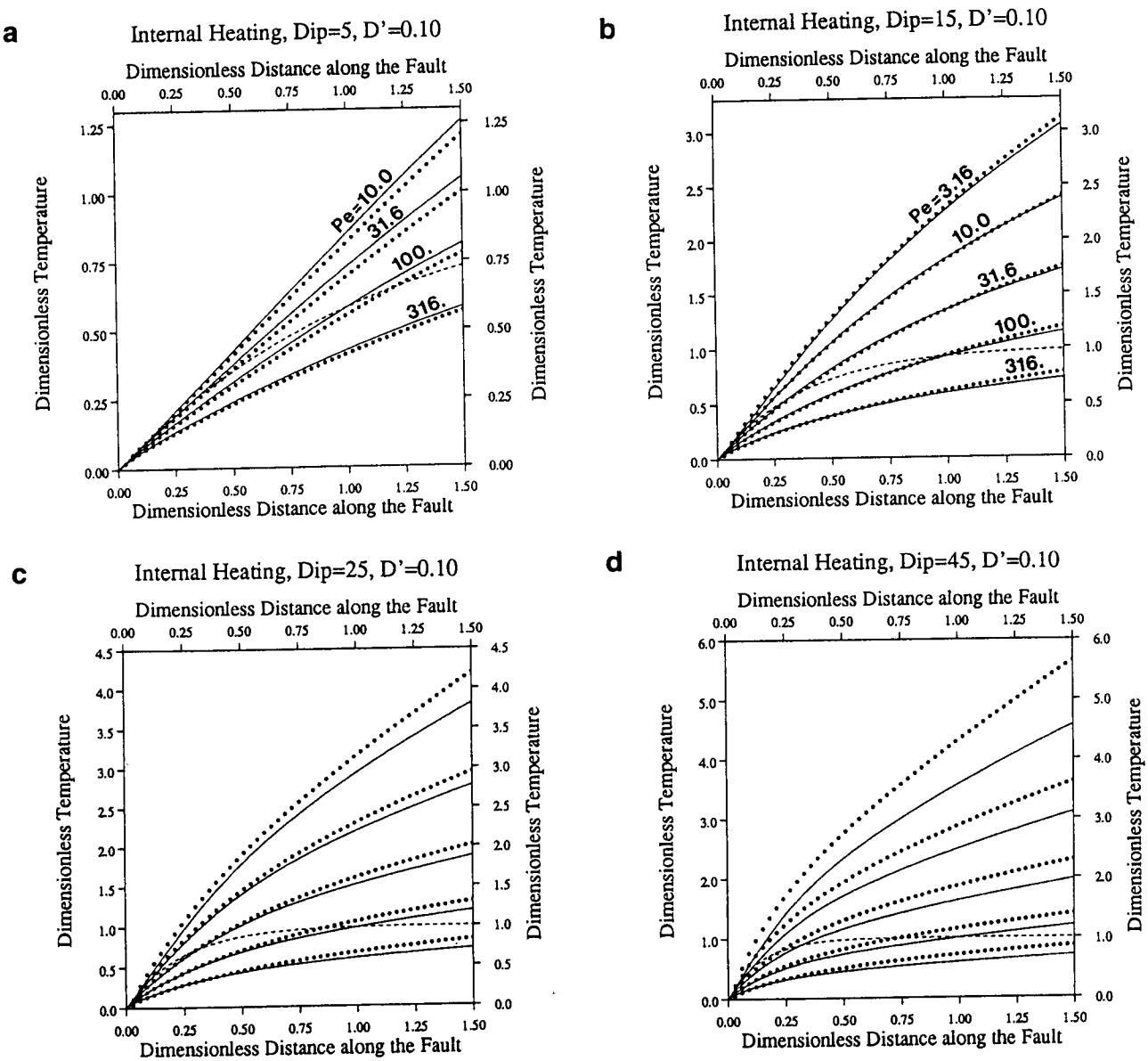

Fig. 8. Plots of dimensionless temperatures against dimensionless distances along the fault for internal heating, with the distribution decreasing exponentially with depth and with the dimensionless scaling depth $D' = 0.10$ or 0.20. The layout and general conclusions are the same as in Figure 4, with the solid lines defined by (19), again with $b = 1$, and with the dashed lines showing the initial temperatures. In all cases, the dimensionless temperature at the base of the lower block has been set equal to unity by choosing the dimensionless heat generation at the surface, A_0', such that $A_0'D' = 1$. Thus, to compare dimensionalized temperatures, those for $D' = 0.20$ should be be multiplied by twice as large a factor as those for $D' = 0.10$.

sum of the time constants in (25) and (26), one can estimate the temperature field with time, sufficiently accurately for most geologic purposes, simply by drawing a smooth curve from the initial value on the fault with a rate of change in time given by (9) or (12) and through 95% of the final steady state value when $t = (t_1 + t_2)$ has transpired, and through the steady state value at $t \geq 2(t_1 + t_2)$.

IMPLICATIONS

Heat Flux at Subduction Zones as a Constraint on Shear Stress

In principle, measurements of heat flux between deep-sea trenches and their adjacent volcanic arcs can be used to place a constraint on the shear stress on the main thrust fault where subduction occurs. We examine this here, but because very few heat flow measurements have been made in such localities, better measurements in the future not only will allow tighter limits on the shear stress than we offer here, but might also reveal our inferences to be in error. The possibility that measurements of conductive heat flow inaccurately represent the total heat loss in such regions is our particular concern.

The typical measured conductive heat flux between trenches and volcanic arcs is about 40 mW m^{-2} or less [*Henry and Pollack*, 1988; *Uyeda and Horai*, 1964; *Watanabe et al.*, 1977]; the distances from the trench to the sites of the measurements range from less than

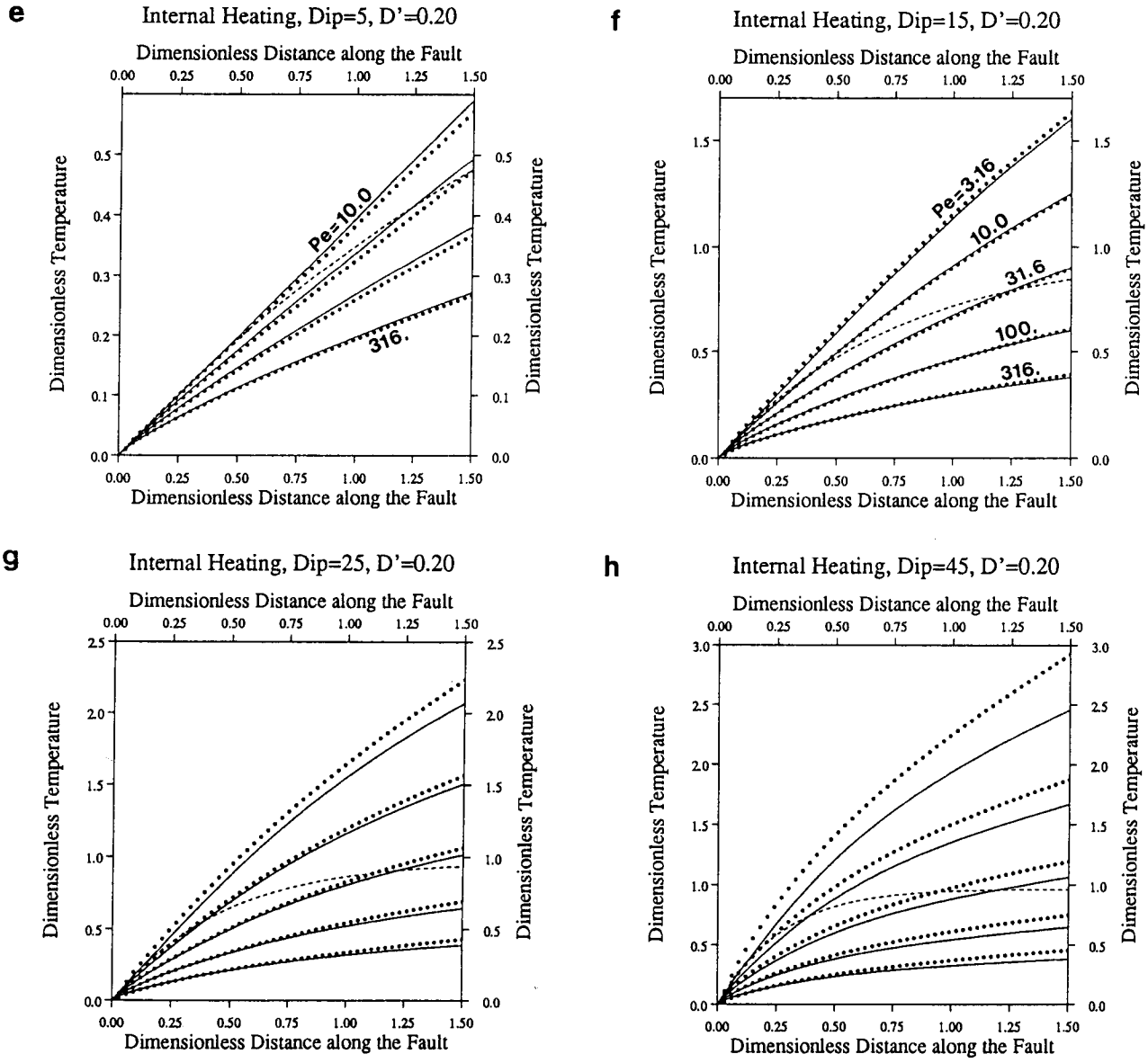

Figure 8. Continued

100 km to 200 km (Table 4). Fault plane solutions of shallow earthquakes, which occur on the thrust fault at subduction zones and whose locations define that fault, indicate dips of roughly 10°–25°. At distances of 75–150 km from trenches, depths of well constrained hypocenteres typically are 25–75 km (Figure 12) [e.g., *Chinn and Isacks*, 1983; *Ekström and Engdahl*, 1989; *Hasegawa et al.*, 1983; *Isacks and Barazangi*, 1977; *Ishida and Hasemi*, 1988; *Obara and Sato*, 1988; *Schwarz et al.*, 1989; *Seno and Takano*, 1989]. For the subduction zones we consider, the depths to the main thrust fault seem to be in this range of 25–75 km (Table 4).

For subduction zones around the Pacific, where rates of subduction are typically about 80–110 mm/yr, the thermal regime of the overlying plate is almost surely in steady state. Subduction has occurred for tens of millions of years, and the time constants in (25) and (26) for $z_f = 75$ km or less, for $V \simeq 100$ mm/yr, and for $u_f \simeq 100$ km, are $t_1 = u/V = 1$ m.y., and $t_2 = z^2/(\pi^2\kappa)$ ≤ 20 m.y. Thus we can use the steady state solutions for the temperature distribution along the fault, given by (15) and (21). Radioactive heat generation in oceanic lithosphere is small, as probably is that in the wedge of overriding lithosphere at subduction zones. Thus, let us neglect radioactivity, and for the purposes here, let us assume that hydrothermal circulation does not carry heat away. Using heat flux $Q = K\partial T/\partial z$, and differentiating (23), we have

$$Q = [Q_0 + \sigma V]/S \tag{28}$$

which yields

$$\sigma = [SQ - Q_0]/V \tag{29}$$

Assuming that Q_0 can be given by the measured heat flux in the area seaward of the subduction zone, and using the various parameters from subduction zones where heat flow has been measured [*Henry and Pollack*, 1988; *Uyeda and Horai*, 1964], calculated shear stresses are

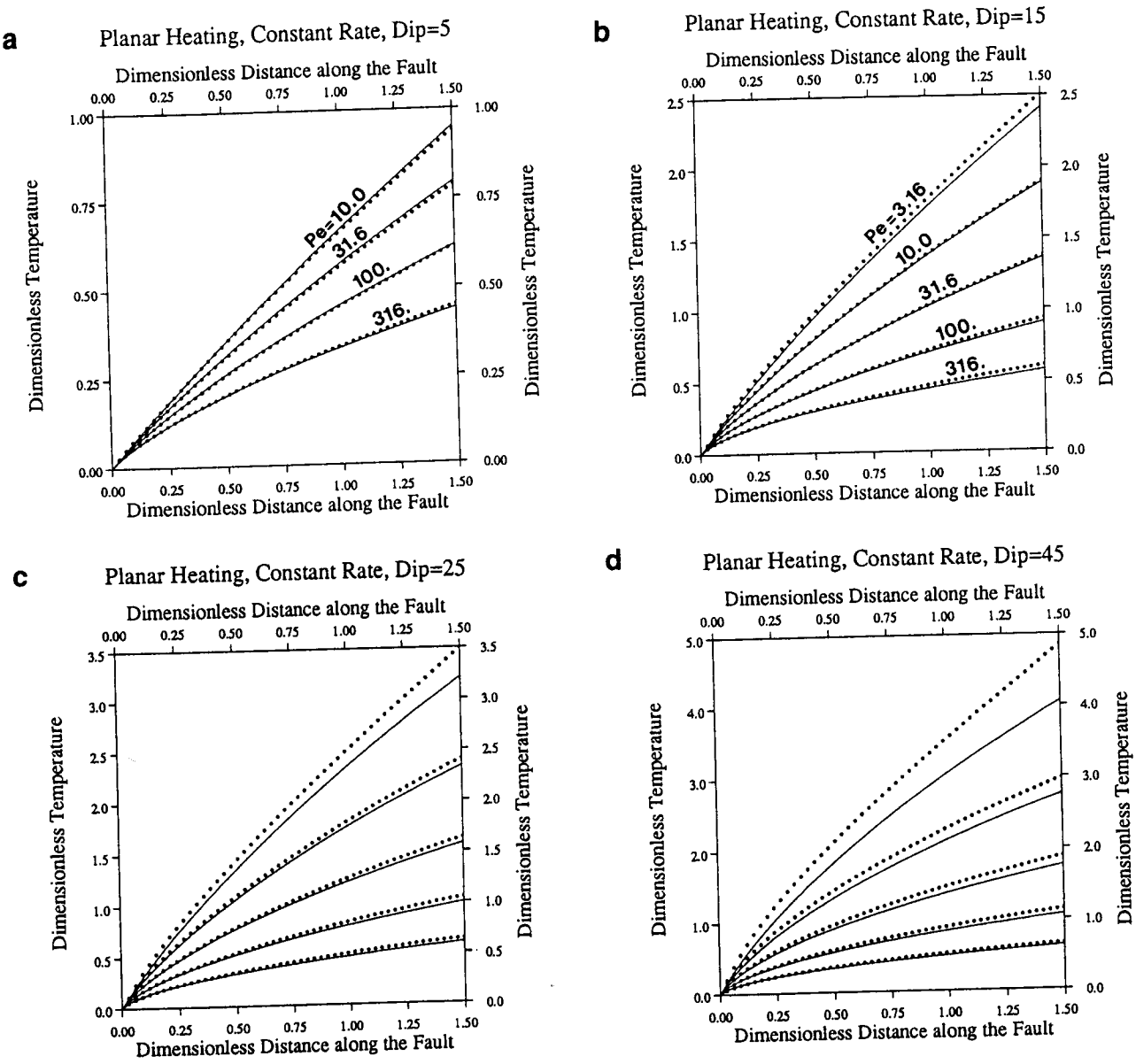

Fig. 9. Plots of dimensionless temperatures against dimensionless distances along the fault for planar heating on the fault at a constant rate, due to shear heating at a constant stress. The layout and general conclusions are the same as in Figure 4, with the solid lines defined by (21), with $b = 1$. The product of the dimensionless stress and the Peclet number is the same so that rate of heating on the fault is the same for all cases: $\sigma' \mathrm{Pe} = 9.723$.

less than 100 MPa, but larger than 30 MPa (Table 4). The uncertainties are sufficiently large, however, especially with the neglect of radioactive heat generation and hydrothermal circulation, that shear stresses larger than 100 MPa or smaller than 30 MPa cannot be ruled out at present.

Heat Sources Responsible for the Anatectic Granitoids in the Himalaya

Tertiary granites crop out widely along the high Himalaya and in southern Tibet, above the Main Central Thrust zone [e.g., *Le Fort*, 1986, 1988], and high initial strontium, neodymium, and lead ratios and $\delta^{18}O$ values attest to their being crustal melts [*France-Lanord et al.*, 1988; *Le Fort et al.*, 1987; *Vidal et al.*, 1982]. *Le Fort* [1981, 1986] argued that water, extracted from the footwall of the Main Central Thrust, lowered the melting temperature of the relatively dry hanging wall. Let us consider the conditions necessary for temperatures to reach 600°C or 650°C along the thrust zone at depths of 30–35 km in the crust.

First note that if the measured heat flow and heat generation in northern India (Table 6, this paper and *Rao et al.*, [1976]) were representative of that of the rock in the Himalaya before thrust faulting began, then, for thermal conductivity of 2.5 W $m^{-1}K^{-1}$, the initial temperatures at 30 km and 35 km would have been 580°C and 660°C, respectively. Thus the difference between intitial and final temperatures need not have been large; slip would have caused an initial decrease in tempera-

TABLE 3. Values of the Coefficient b in (16) Inferred From the Numerical Experiments.

	Peclet number				
	3.16	10.0	31.6	100	316
$\delta = 5°$					
Heating from below	0.93	1.01	1.04	1.02	0.99
Internal heating, $D' = 0.1$	-	1.20	1.17	1.12	1.07
Internal heating, $D' = 0.2$	-	1.12	1.12	1.08	1.04
Planar heating, $\sigma = \text{const}$	-	1.03	1.04	1.02	0.98
Planar heating, $\sigma = \mu z$	-	1.10	1.33	1.33	1.32
$\delta = 15°$					
Heating from below	0.90	0.97	0.97	0.98	0.95
Internal heating, $D' = 0.1$	.94	1.01	1.03	1.02	0.99
Internal heating, $D' = 0.2$	.88	1.01	1.03	1.02	1.00
Planar heating, $\sigma = \text{const}$	.89	0.97	0.99	0.98	0.95
Planar heating, $\sigma = \mu z$	0.80	1.17	1.31	1.33	1.33
$\delta = 25°$					
Heating from below	0.88	0.94	0.96	0.96	0.95
Internal heating, $D' = 0.1$	.82	0.93	0.95	0.95	0.94
Internal heating, $D' = 0.2$	.80	0.93	0.97	0.97	0.97
Planar heating, $\sigma = \text{const}$	.83	0.94	0.96	0.96	0.94
Planar heating, $\sigma = \mu z$	0.70	1.10	1.25	1.31	1.33
$\delta = 45°$					
Heating from below	0.76	0.86	0.90	0.91	0.90
Internal heating, $D' = 0.1$	.68	0.81	0.85	0.87	0.85
Internal heating, $D' = 0.2$	.69	0.84	0.88	0.90	0.92
Planar heating, $\sigma = \text{const}$	.72	0.89	0.92	0.93	0.94
Planar heating, $\sigma = \mu z$	0.50	0.95	1.16	1.26	1.33

ture near the fault, but shear heating and radioactivity could have later provided the heat for the temperatures to return to approximately their initial values.

We may ask two separate questions. First, what level of shear stress would be required for the steady state temperature during slip on the fault to be no lower than the temperature at the same level before slip began? The second question is: What shear stress is necessary for the temperature at 30 or 35 km to reach 600° or 650°C during slip on the fault, regardless of the temperature before slip began?

All temperatures calculated from measurements of heat flux and radiogenic heat production are inversely proportional to the coefficient of thermal conductivity, K, which for the crust is uncertain by at least 20%. The first of these questions can be answered without making an estimate of conductivity, but the second cannot.

To make the answer to the first question clearer, we begin with a simplification. Because the depth of 30 km exceeds 2 D ($\simeq$ 28 km), we can neglect terms with the factors $e^{-z/D}$ and $e^{-a/D}$ in (A1), and the expression for the initial temperature (A1) becomes:

$$T(z_f, 0) = [Q_0 z_f + A_0 D^2]/K \tag{30}$$

With similar simplifications, the steady state temperature on the fault, from (15), (19), and (21), is

$$T_f(z_f) = [Q_0 z_f + A_0 D(D + z_f) + \sigma V z_f]/KS \tag{31}$$

Ignoring the terms with factors of $e^{-z/D}$ amounts to neglecting about 15°C.

Equating the initial and steady state temperatures yields a condition for the magnitude of σ necessary for the temperature on the fault, after it drops initially, to return to its original value

$$\begin{aligned} \sigma &= \left[Q_0\sqrt{z_f V \sin\delta/\kappa}\right. \\ &+ \left. A_0 D[D\sqrt{z_f V \sin\delta/\kappa}/z_f - 1]\right]/V \end{aligned} \tag{32}$$

It turns out that the particular range of plausible values of z_f, V, δ, and D allow the second term in (32) to be ignored. When melting occurred, the distance of the zone of melting from where the fault reached the Earth's surface must have been at least 100 km, approximately the present distance from the granites to the southernmost trace of the Main Central Thrust. If that distance were 120 km, then for $z_f \leq 35$ km, $\delta \leq 17°$. In the other extreme, if the hanging wall of the Main Central Thrust has undergone 50% horizontal shortening [*Johnson*, 1986], then for $z_f = 30$ km and $u_f \simeq 210$ km, $\delta \simeq 8°$. The rate of slip probably was comparable with the present rate of 15 ± 5 mm/yr, but might have reached 25 mm/yr. At 15 mm/yr, an approximately steady state regime would have been approached by roughly 15–20 m.y. For $\delta = 12°$ (± 4°), $z_f = 30$–35 km, and $V = 15 \pm 5$ mm/yr, the factor $\sqrt{z_f V \sin\delta/\kappa} \simeq 1.8$ (±0.6) (Table 5), and for $D \simeq 14$ km, $D/z_f \simeq 0.4$–0.5. Hence, the bracketed factor in the second term in (26) is very small, ($\simeq -0.1$), and neglecting the entire second term, we have

$$\sigma \simeq Q_0\sqrt{z_f \sin\delta/V\kappa} \tag{33}$$

which overestimates σ in (32) by less than 10%. For $Q_0 = 38$ mW m^{-2}, $V = 15$ mm/yr and $\delta = 12°$, $\sigma \simeq 140$ MPa, but for $V = 20$ mm/yr and $\delta = 8°$, $\sigma \simeq 100$ MPa, and for 10 mm/yr and 16°, $\sigma \simeq 190$ MPa. Thus, if melting occurred by the temperature first dropping from an initially high value then returning to that value later, the shear stress must have been nearly 100 MPa, if it did not exceed that amount.

To answer the second question we may apply (24) directly to calculate the steady state temperature on the fault, which reduces to

$$\sigma = [KST_f - Q_0 z_f - A_0 D(D + z_f)]/V z_f \tag{34}$$

Using the values of A_0 and D given in Table 6 and the other parameters discussed above, the shear stress needed for the temperature to reach 650°C at 30 or 35

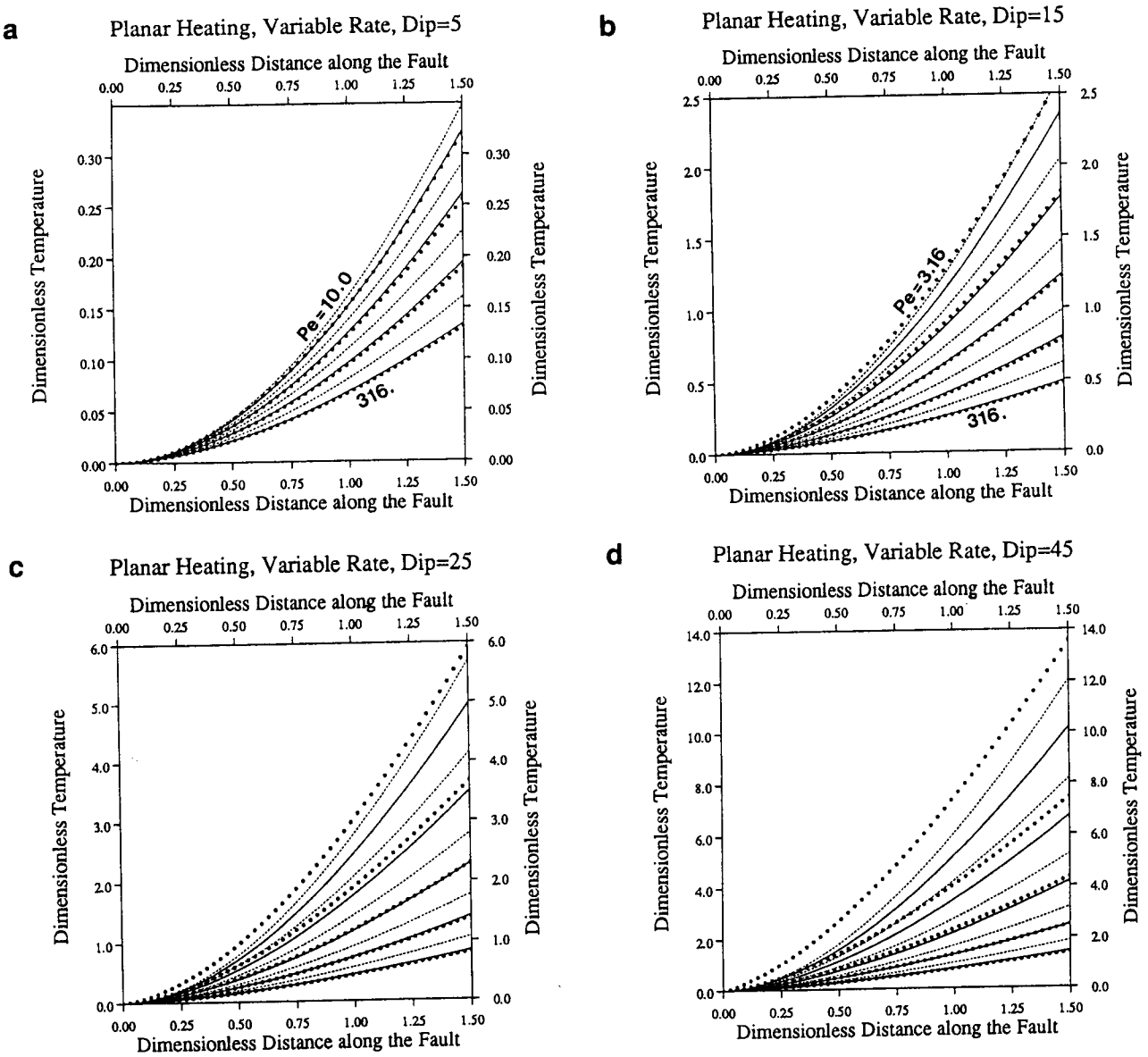

Fig. 10. Plots of dimensionless temperatures against dimensionless distances along the fault for planar heating on the fault at an increasing rate, due to shear heating associated with a stress increasing linearly with depth. The layout and general conclusions are the similar to those in Figure 4, but the solid lines are given by (22) with $b = 1.3$, as theory suggests, and dashed lines show curves with $b = 1$. Note that $b = 1$ fits poorly, except for the data in (b), for which Pe = 3.16. In this case the assumption of negligible lateral transfer of heat probably is not a good one. As in Figure 6, the product of the dimensionless stress and the Peclet number is the same so that rate of heating on the fault is the same for all cases: this was accomplished by setting μ' Pe = 31.6.

km would exceed 100 MPa for nearly all of the plausible range of parameters, and could exceed 200 MPa for high slip rates and steep faults. Only for relatively gentle dips, $\delta \leq 10°$, and relatively high rates, $V \geq 15$ mm/yr, could the calculated shear stress be less than 100 MPa, and even then no smaller than about 75 MPa. For instance, for $\delta = 8°$, $z_f = 30$ km, and $V = 15$ mm/yr, $\sigma = 90$ MPa, but for $\delta = 10°$, $z_f = 35$ km, and $V = 20$ mm/yr, $\sigma = 110$ MPa. Moreover, note that the values of Q_0 and A_0 given by *Rao et al.* [1976] are typical of continental regions, but relatively large for shields. (The value for D is also quite large, but its value has a small effect in (34).) If typical values of Q_0 and A_0 for shields, roughly two thirds those given by *Rao et al.* [1976], were used, then the calculated stresses would be roughly 50% larger than those given above and would certainly exceed 100 MPa.

Maximum Depths of Earthquakes as Bounds on the Shear Stress in Continents

Earthquakes in continental crust seem to be confined to depths where the temperature is less than

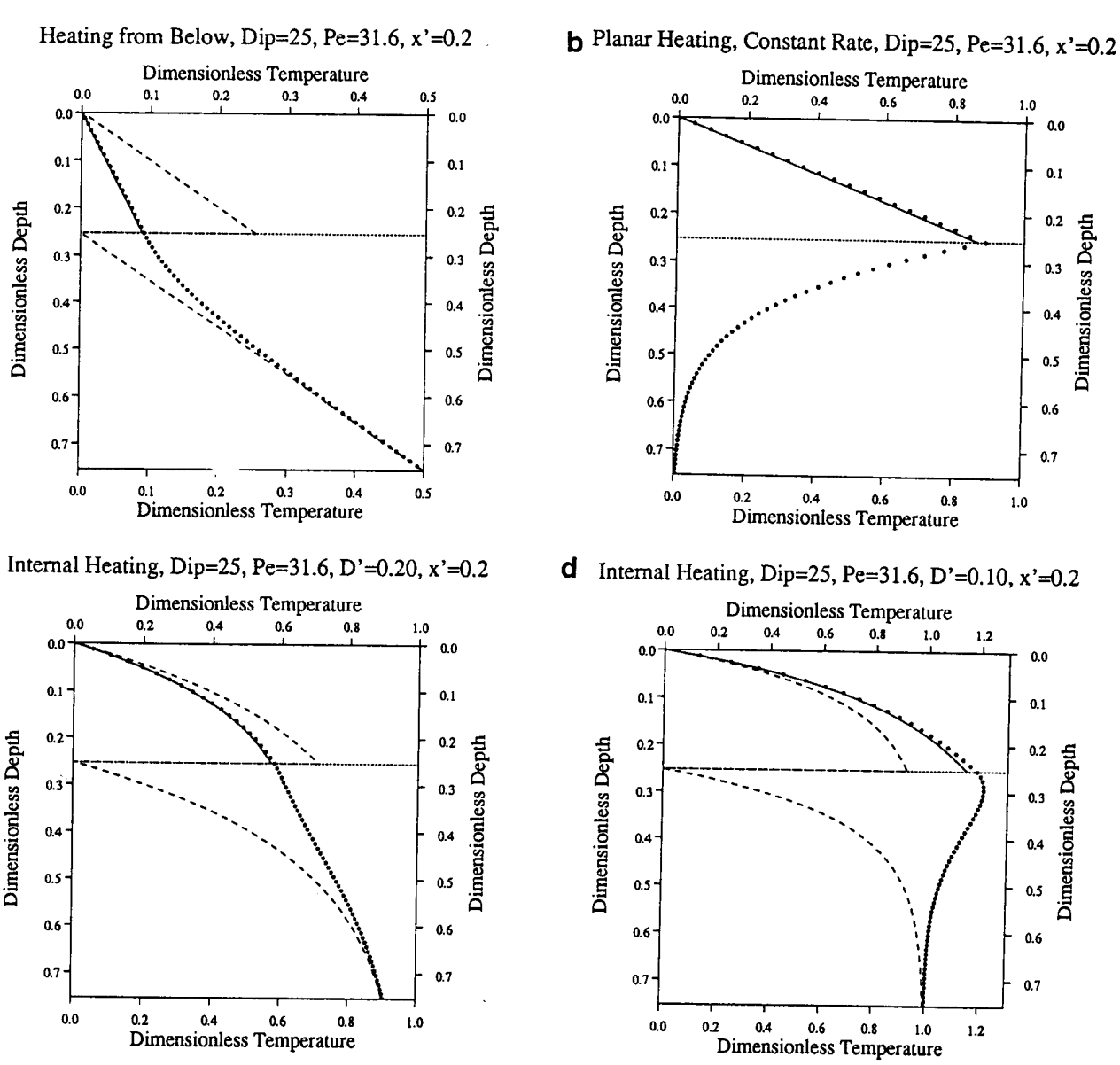

Fig. 11. Profiles of initial (dashed lines) and steady (solid lines) temperatures through the upper block at $x' = 0.2$ and the lower block at $u' = 0.2$ for (a) heating from below the lithosphere, (b) planar heating at a constant rate (shear heating at a constant stress) and (c) and (d) internal (radiogenic) heating with two values of D'. Dots show experimentally determined temperatures at each gridpoint and solid lines show temperatures in the upper block calculated from (24) with the appropriate heat sources.

350° ± 100°C [*Chen and Molnar*, 1983; *Meissner and Strehlau*, 1982; *Sibson*, 1982]. Let us consider what constraints this observation puts on shear stresses at rapidly slipping thrust faults. For instance, moderate-sized earthquakes showing thrust faulting on gently dipping planes in the Himalaya occur at depths of about 15 km, and apparently not deeper than about 18 km [*Baranowski et al*, 1984; *Molnar and Lyon-Caen*, 1989; *Ni and Barazangi*, 1984]. For the parameters in Table 6, with $u_f = 100$ km, $V = 15 \pm 5$ mm/yr, $z_f = 18$ km, and therefore $\delta = 10°$, we obtain $S = 2.2$ (± 0.2). To estimate σ for $T_f = 350 \pm 100$°C at $z_f = 18$ km, let us ignore terms in $e^{-a/D}$, but use the rest of (24), because z_f is not much larger than D. Instead of (34), we have

$$\sigma = \left[KST_f - Q_0 z_f - A_0 D[D + z_f][1 - e^{-z_f/D}]\right] / V z_f \quad (35)$$

For the temperature along the fault to reach 350 °C, the shear stress, σ, must reach 77 (± 10) MPa, and for it to reach 450°C σ must be 140 MPa. As noted above, if the values of both Q_0 and A_0 were 33% smaller, the calculated stresses would be about 50% larger.

CONCLUSIONS

Both simple theoretical arguments and numerical experiments show that the advection of heat downward along a thrust fault by the movement of the lower block reduces, by the divisor in (16), the temperature field

TABLE 4. Measured Dips, Depths, and Heat Fluxes at Subduction Zones and Inferred Shear Stresses

	Q, mW m^{-2}	Q_0, mW m^{-2}	V, mm/a	x_f, km	z_f, km	δ, deg	S	σ, MPa
Japan	34 ± 4	50 ± 15	105 ± 10	205 ± 10	70 ± 10	19 ± 3	9.7 (± 1.0)	84 (± 18)
	32 ± 3	50 ± 15	105 ± 10	170 ± 10	60 ± 10	19 ± 4	9.2 (± 1.3)	73 (± 17)
Peru	33 ± 5	(60)	80 ± 5	85 ± 10	30 ± 5	20 ± 5	6.1 (± 1.6)	55 (± 24)

Q, measured heat flux between trenches and island arcs. The values for Japan and the Kuriles were taken from *Uyeda and Horai* [1964], those for Peru from *Henry and Pollack* [1988].
Q_0, heat flux to the base of the lithosphere. For Japan the measured values seaward of the trench were used, and for Peru, we assumed a value of 60 mW m^{-2} appropriate for oceanic lithosphere with an age of 40 Ma [*Parsons and Sclater*, 1977].
V, rate of subduction. The values were calculated from angular velocities given by *Minster and Jordan* [1978].
x_f, distance of heat flux measurements from the trench axis. For Japan we measured distances from plots in *Uyeda and Horai* [1964]; and we took those in Table 1 of *Henry and Pollack* [1988] for Peru.
z_f, depth of the subduction zone below sites of heat flux measurements. For Japan we measured the depths given in profiles of seismicity by *Seno and Takano* [1989], *Obara and Sato* [1988] and *Hasegawa et al.* [1983]; for Peru we used the profiles of *Isacks and Barazangi* [1977].
$S = 1 + \sin\delta\sqrt{V u_f/\kappa}$, where $u_f = \sqrt{x_f^2 + z_f^2}$ and $\delta = \tan^{-1} z_f/x_f$ is dip of subduction zone.
σ is estimated shear stress on the thrust fault.

along the fault below what it would be in the absence of advection. For heating from below, radiogenic heating, and shear heating at constant stress, the factor b in (16) is essentially unity (Table 3), as suggested by theoretical arguments. These results imply that for sufficiently large rates of underthrusting, greater than about 1 mm/yr, lateral conduction of heat is not important compared with advection along the fault or diffusion in the vertical direction, as noted by Ruppel et al. [1988]. Simple formulae describe the steady state temperature field in the upper block (equation (24), and the heat flux through it (e.g., equation (28)). Thus, sophisticated numerical modeling of steady state temperatures is unlikely to be scientifically revealing.

Numerical experiments also corroborate simple expressions for the change in temperatures at short times after the initiation of thrust faulting, equations (9), (10), and (12). Deviations from these rates of temperature change become significant after elapsed times have

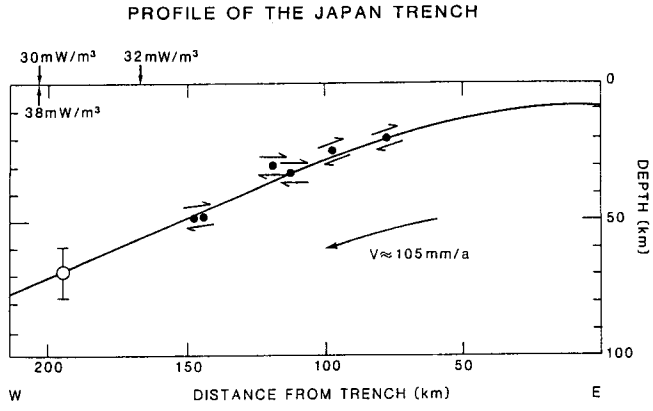

Fig. 12 Profile across the Japan trench, showing positions of moderate earthquakes whose depths and fault plane solutions are well constrained [*Seno and Takano*, 1989], and the positions of heat flow measurements [*Uyeda and Horai*, 1964]. The approximate plate boundary, and its uncertainty, are defined by the hypocentral locations of *Hasegawa et al.* [1983], *Ishida and Hasemi* [1988] and *Obara and Hasegawa* [1988].

TABLE 5. Values of $\sqrt{z_f V \sin\delta/\kappa}$ for Plausible Values of z_f, V and δ near the Main Central Thrust in the Himalaya.

V	10 mm/a		15 mm/a		20 mm/a	
z_f	30 km	35 km	30 km	35 km	30 km	35 km
8°	1.15	1.25	1.41	1.52	1.63	1.76
10°	1.29	1.39	1.58	1.70	1.82	1.97
12°	1.41	1.52	1.73	1.86	1.99	2.15
14°	1.52	1.64	1.86	2.01	2.15	2.32
16°	1.62	1.75	1.99	2.15	2.29	2.48

TABLE 6. Values of Parameters Used in Calculating Shear Stresses During Motion on the Main Central Thrust

Parameter	Value	Reference
Q_0	38 mW m^{-2}	*Rao et al., 1976*
A_0	2.5 μW m^{-3}	*Rao et al., 1976*
D	14 km	*Rao et al., 1976*
K	1.5–2.5 W m^{-1}K^{-1}	
V	10–25 mm/yr	*Lyon-Caen and Molnar, 1985*

exceeded the shorter of two basic time constants: the time for the Earth's surface to reach the point along the fault in question, t_1, equation (25), and the time constant for diffusion of heat into a layer with its thickness equal to the depth of the fault at the point in question, t_2, equation (26). Steady state temperatures are approached when the elapsed time exceeds the sum of these time constants and is essentially reached when the time exceeds twice that sum.

At subduction zones, where rates of underthrusting are rapid, advection carries a large amount of heat downward, yet the typical measured surface heat fluxes between the trenches and the volcanoes are 25–40 mW m^{-2} — higher than could be supported by conduction from the subducting plate alone. If such fluxes are accurate measures of the heat leaving the surface of the upper block, and if radiogenic heating is small in the overriding plate, then dissipative heating must be large, and shear stresses must approach 100 MPa.

Similarly, to generate granitoid magmas near the Main Central Thrust, even at relatively low temperatures of 600° to 650° C, in rocks initially not hotter than 700°C, while underthrusting at a rate of 15 ± 5 mm/yr occurs, requires a large heat source. Heating from below the lithosphere and radiogenic heating within the crust are insufficient to prevent the temperature near the Main Central Thrust from dropping hundreds of degrees as advection carries heat away rapidly. Dissipative heating with shear stresses of roughly 100 MPa, or more, seem to be the only plausible source of additional heat.

If moderate earthquakes (5.5 ≤ magnitude ≤ 7) occur at depths no greater than 18 km in the Himalaya because temperatures exceed 350°C along the fault at that depth [e.g., *Chen and Molnar*, 1983], then shear stresses of nearly 100 MPa are necessary to raise the temperature to such a value at that depth.

Thus, to the embarrassment of the first of us, we conclude that shear stresses approaching, if not exceeding, 100 MPa commonly resist slip on major thrust faults in the Earth, as numerous others before us, using different data or different logic, have also concluded.

APPENDIX A. DETAILS OF THE METHOD OF SOLVING THE HEAT FLOW EQUATION

We solved separately the heat flow equation in the upper and lower blocks, defined in Figure 1. We used the coordinates (x, z) in the top block, parallel and perpendicular the Earth's surface, and (u, w) in the lower block, parallel and perpendicular to the interface between them, the fault surface. The fault surface is defined by $\tan\delta = z/x$ or by $w = 0$.

Initial conditions. For the case of heating from below, initially $T(x, z, 0) = Q_0 z/K$ in the upper block, which in dimensionless form is $T' = z'$. In the lower block beneath the region not overlain by the upper block, $T(u, w) = Q_0 w/K$, or $T' = w'$, and in the region beneath the upper block $T(u, w, 0) = Q_0 Z(u, w)/K$, or $T' = Z'$, where $Z'(u', w') = u' \sin\delta + w' \cos\delta$. We joined isotherms defined by these expressions along the line $w = u \tan\delta/2$. For cases with radioactivity as the heat source, we considered heat generation decreasing with depth according to $A(z) = A_0 e^{-z/D}$, with the initial temperature field given by that for steady state without a flux from below

$$T(x, z, 0) = \frac{A_0 D^2}{K}\left[1 - e^{-z/D}\right] - \frac{A_0 D z}{K} e^{-a/D} \quad \text{(A1)}$$

In the lower block, for the area not beneath the upper block, we used the same expressions, with w substituted for z, and for the area beneath the upper block, as before, we used $Z(u, w)$ in place of z. For shear heating, calculations began with a zero temperature field throughout the region.

Boundary conditions. On the top of the upper block, $T'(x', 0) = 0$, or $T(x, 0) = 0$, and on the side there is no flux of heat across this surface, $\partial T/\partial x = 0$. For the lower block, there is no flux across the sides, $\partial T/\partial u = 0$. Because we considered times short compared with the thermal time constant of the lithosphere, in practice we applied a constant flux Q_0 at the base simply by fixing the temperature at the base, $w = a$, to be its initial temperature; this provided the equivalent of a constant flux for all values of Pe and z_f we considered. For radioactive or shear heating, the boundary condition at the base was one of no heat flux across it.

We dealt with the relative motion of the blocks simply by taking the temperature at each grid point along the fault to be the average of the temperatures calculated for that point in each block. Diffusion of heat between the blocks was handled by attaching fictitious rows of grid points to the top of the lower block and the bottom of the upper block. We interpolated and assigned temperatures to these fictitious points from the temperatures calculated in the other of the blocks, and used them as boundary conditions in the diffusion calculation for the respective blocks. For enough grid points along the fault and short enough time steps (defined below), the temperatures along the fault calculated in the two blocks differed from each other by less than 0.5% for each time step. This procedure was repeated for each time step, such that new positions and new temperatures of the fictitious points were calculated each time.

Finite difference algorithm. The upper block was divided into $N + 1$ evenly spaced rows and $N + 1$ evenly spaced columns such that the coordinates (x', z') were specified by (i, j) and the fault was defined by $i = j$. The lower block consisted of $N_W + 1$ evenly spaced rows and $N + N_L + N_R + 1$ evenly spaced columns of points, where N_L and N_R are the number of columns to the left and right of the upper block. In all cases N_W was chosen equal to N and $N_L = N_R = N/10$. Note that the spacings between grid points in the x-, z-, u-, and w-directions are not equal. The spacings between rows

and columns in the upper block were such that distances between points along the fault are $3a/N$.

We attempted to take advantage of the stability to large timesteps of the Alternate-Direction-Implicit (ADI) finite-difference algorithm [*Press et al.*, 1986]. The temperature is fixed, however, at three of the four points surrounding the corner of the upper block and the finite difference approximation becomes explicit in the z-direction there. We were constrained therefore to carry out calculations with the dimensionless timestep, $\Delta t'$, for each pair of ADI passes set at less than $\Delta z'^2$, where $\Delta z'$ is the dimensionless step in the z-direction of the upper block. A more sophisticated treatment of the condition at the corner would probably be desirable, if computer time were costly.

In addition to this condition, the duration of the time step was governed by the spacing of grid points along the fault, by the dip of the fault, and by the rate of slip. The lower block advances a distance $V\Delta t$ with each time step, and that distance must not exceed the spacing, Δu, of grid points. To ensure accuracy in the diffused heat flux, that distance did not exceed $0.1\Delta u$. To effect this, we chose an integer $n = \Delta u/(V\Delta t) = 3/(N\mathrm{Pe}\Delta t')$, so that after every n time steps, the grid points along the interface between the upper and lower blocks would be aligned. This choice of $n(\geq 10)$ then dictated the duration of the dimensionless time step

$$\Delta t' \leq \frac{3}{Nn\mathrm{Pe}} \tag{A2}$$

In practice, the condition that $\Delta t' \leq \Delta z'^2$ was usually more restrictive.

Tests. We used four separate programs for the different heat sources, but each used the same routines for solving the diffusion equation. We tested those routines by comparing the calculated temperatures with those for which analytic solutions could be found. For both the wedge-shaped upper block and the rectangular lower block, we imposed instantaneous changes in temperature at the edges and compared the calculated temperatures near the edges of the blocks at short times with the analytical solution, given in terms of an error function, appropriate for the temperature within a half-space after an instantaneous change on the boundary [*Carslaw and Jaeger*, 1959, p. 63]. Differences of less than 0.1% were obtained when N = 100. For the rectangular lower block, we compared calculated temperatures at longer elapsed times with those appropriate for the warming of a rectangle for which the temperature on the perimeter was instantaneously changed [*Carslaw and Jaeger*, 1959, chap. 5]. Again for $N = 100$, differences were less than 0.1%. These tests suggest that for these simple cases the results are accurate to such a percentage.

In order to evaluate the convergence of the calculated temperatures, we examined calculated temperatures for runs with $\delta = 15°$ and Pe = 31.6, using a variety of values of N, equal to 20, 50, 100, and 200. Calculated temperatures with $N = 50$ and 100 and with $N = 100$ and 200 differed from one another by less than 1%, and in most cases by less than 0.3%. Moreover, the latter differences were smaller than the former by between 1.5 and 2 times. From this we conclude that the finite difference scheme converged. For all runs shown, we used $N = 100$.

Appendix B. Temperatures Within a Semi-Infinite, One-Dimensional Medium With the Temperature on Its End Increasing With Time

We examine the temperature in a semi-infinite one-dimensional medium, as an analogy for the temperature in a section in the lower block of a thrust fault and perpendicular to the fault, as the block slides beneath an upper block whose temperature field has reached steady state. The temperature on the fault must increase with depth, and therefore any point on the top surface of the lower block will be placed in contact with material at successively higher temperatures. This analogy is appropriate when lateral conduction of temperature is small compared with that in the direction perpendicular to the fault.

Consider a temporal increase of the temperature at the surface of the one-dimensional medium, $y \geq 0$, of the form: $T(0,t) = \alpha t^{m/2}$, where m is an integer. Obviously, for $m = 2$, the temperature increases linearly with time. *Carslaw and Jaeger* [1959, p. 63] give the solution to the one-dimensional heat-flow equation for such a condition:

$$T(y,t) = \alpha t^{m/2}\Gamma(m/2+1)2^m \mathrm{i}^m\mathrm{erfc}\frac{y}{2\sqrt{\kappa t}} \tag{B1}$$

where $\mathrm{i}^m\mathrm{erfc}(x)$ is the mth integral of the complementary error function.

As discussed in the text, we consider the temperature gradient within such a one-dimensional medium:

$$\frac{\partial T}{\partial y} = -\frac{\alpha t^{m/2}\Gamma(m/2+1)2^{m-1}}{\sqrt{\kappa t}}\mathrm{i}^{m-1}\mathrm{erfc}\frac{y}{2\sqrt{\kappa t}} \tag{B2}$$

At the surface, $y = 0$, this becomes

$$\frac{\partial T}{\partial y} = b\frac{\alpha t^{m/2}}{\sqrt{\kappa t}} \tag{B3}$$

or

$$\frac{\partial T}{\partial y} = -b\frac{T(0,t)}{\sqrt{\kappa t}} \tag{B4}$$

where we have used

$$\mathrm{i}^m\mathrm{erfc}(0) = \frac{1}{2^{m-1}\Gamma(m/2+1)}$$

[*Carslaw and Jaeger*, 1959, p. 484] and

$$b = \frac{\Gamma(m/2+1)}{\Gamma(m/2+1/2)} \tag{B5}$$

Note that for $n = 1, 3/2, 2, 5/2$, and 3, $\Gamma(n) = 1, \sqrt{\pi}/2,$

1, $3\sqrt{\pi}/4$, and 2. For $m = 1$, 2, 3, and 4, $b = \sqrt{\pi}/2 = 0.886$, $2/\sqrt{\pi} = 1.128$, $3\sqrt{\pi}/4 = 1.329$, and $8/3\sqrt{\pi} = 1.505$.

Thus, for this class of temporal variation, $T(0,t) = \alpha t^{m/2}$, the gradient, and hence the heat flux, are proportional to the ratio of the temperature on the surface at any time to $\sqrt{\kappa t}$.

Acknowledgments. We thank A. Simmins for help with computing problems, Hiroo Kanamori for directing us to studies of seismicity in Japan, Göran Ekström and Susan Schwarz for providing preprints of papers in press, and A. Lachenbruch, R.C. Liebermann, and an anonymous reviewer for prompt, constructive criticism of the manuscript. This work was supported by a Royal Society Guest Research Fellowship to Peter Molnar, and by NERC grant GR3/7032 and NSF grant 8500810-EAR.

REFERENCES

Arita, K., Origin of inverted metamorphism of the lower Himalaya, Central Nepal, *Tectonophysics*, *95*, 43–60, 1983.

Baranowski, J., J. Armbruster, L. Seeber, and P. Molnar Focal depths and fault plane solutions of earthquakes and active tectonics of the Himalaya, *J. Geophys. Res.*, *89*, 6918–6928, 1984.

Barton, C.M., and P.C. England, Shear Heating at the Olympos (Greece) thrust and the deformation properties of carbonates at geological strain rates, *Geol. Soc. Am. Bull.*, *90*, 483–492, 1979.

Bickle, M.J., C.J. Hawkesworth, P.C. England, and D.R. Athey A preliminary thermal model for regional metamorphism in the eastern Alps, *Earth Planet. Sci. Lett.*, *16*, 13–28, 1975.

Bird, P., Initiation of intra-continental subduction in the Himalaya, *J. Geophys. Res.*, *83*, 4975–4987, 1978.

Brace, W.F., and D.L. Kohlstedt, Limits on lithospheric stress imposed by laboratory experiments, *J. Geophys. Res.*, *85*, 6248–6252, 1980.

Brace, W.F., and J.B. Walsh, SOme direct measurements of the surface energy of quartz and orthoclase, *Am. Mineral.*, *47*, 1111–1122, 1962.

Brewer, J., Thermal effects of thrust faulting, *Earth Planet. Sci. Lett.*, *56*, 233–244, 1981.

Brune, J.N., and C.R. Allen, A low-stress-drop, low magnitude earthquake with surface faulting: the Imperial, California, earthquake of March 4, 1966., *Bull. Seismol. Soc. Am.*, *57*, 501, 1967.

Brune, J.N., T.L. Henyey, and R.F. Roy, Heat flow, stress, and rate of slip on the San Andreas Fault, California, *J. Geophys. Res.*, *74*, 3821–3827, 1969.

Brunel, M., and J.-R. Kienast, Etudes petro-structurale des chevauchements ductiles Himalayens sur la transversale de l'Everest-Makalu (Nepal oriental), *Can. J. Earth Sci.*, *23*, 1117–1137, 1986.

Carslaw, H.S, and J.C. Jaeger, *Conduction of Heat in Solids*, Oxford University Press, New York, 1959.

Chen, W.-P., and P. Molnar, Focal depths of intracontinental and intraplate earthquakes and their implications for the thermal and mechanical properties of the lithosphere, *J. Geophys. Res.*, *88*, 4183–4214, 1983.

Chinn, D.S., and B.L. Isacks, Accurate source depths and focal mechanisms of shallow earthquakes in western South America and the New Hebides island arc., *Tectonics*, *2*, 529–564, 1983.

Christie, J.M., and A. Ord, Flow stress from microstructures of mylonites: experimental assessment., *J. Geophys. Res.*, *85*, 6252–6262, 1980.

Dalmayrac, B., and P. Molnar, Parallel thrust and normal faulting in Peru and constraints on the state of stress. *Earth Planet. Sci. Lett. 55*, 473–481, 1985.

Deniel, C., P. Vidal, A. Fernandez, P. Le Fort and J.-J. Peucat, Isotopic study of the Manaslu granite (Himalaya, Nepal): inferences on the age and source of Himalayan leucogranites, *Contribs. Mineral. Petrol.*, *96*, 78–92, 1987.

Ekström, G., and R.E. Engdahl, Earthquake source parameters and stress distribution in the Adak Island region of the central Aleutian Islands, Alaska, *J. Geophys. Res.*, *94*, 15499–15519, 1989

England, P. C., Some thermal considerations of the Alpine metamorphism — past, present and future, *Tectonophysics*, *46*, 21–40, 1978.

England, P.C., and A.B. Thompson, Pressure-Temperature-time paths of regional metamorphism I. Heat transfer during the evolution of regions of thickened crust, *J. Petrol.*, *25*, 894–928, 1984.

France-Lanord, C., S.M.F. Sheppard, and P. Le Fort, Hydrogen and Oxygen isotope variation in the High Himalaya peraluminous Manaslu leucogranite: evidence for heterogeneous source., *Geochim. Cosmochim. Acta*, *52*, 513–526, 1988.

Gansser, A., *The Geology of the Himalayas*, Wiley Interscience, New York, 1964.

Graham, C.M., and P.C. England, Thermal regimes and regional metamorphism in the vicinity of overthrust faults: An example of shear heating and inverted metamorphic zonation from southern California, *Earth Planet. Sci. Lett.*, *31*, 142–152, 1976.

Hanks, T.C., Earthquake stress drops, ambient tectonic stresses, and stresses that drive plate motions., *Pure Appl. Geophys.*, *115*, 441–458, 1977.

Hanks T.C. and C.B. Raleigh, The conference on magnitude of deviatoric stress in the Earth's crust and uppermost mantle, *J. Geophys. Res.*, *85*, 6083–6085, 1980.

Hasegawa, A., et al Spatial distribution of earthquakes beneath Hokkaido and northern Honshu, Japan (in Japanese), *Zisin*, *36*, 129–150, 1983.

Henry, S.G., and H.N. Pollack, Terrestrial heat flow above the Andean subduction zone in Bolivia and Peru, *J. Geophys. Res.*, *93*, 15153–15162, 1988.

Henyey, T.L., and G.J. Wasserburg, Heat flow near major strike-slip faults in California, *J. Geophys. Res.*, *76*, 7924–7946, 1971.

Hodges, K.V., P. Le Fort, and A. Pecher, Possible thermal buffering by anatexis of crust in collisional orogens: Thermobarometric evidence from the Nepalese Himalaya, *Geology*, *18*, 707–710, 1988.

Hubbard, M.S., Thermo-barometric constraints on the thermal history of the Main Central Thrust zone and the Tibetan slab, Eastern Nepal, Himalaya, *J. Metamorph. Petrol.*, *7*, 19–30, 1989.

Hubbard, M.S. and T.M. Harrison, $^{40}Ar/^{39}Ar$ constraints on deformation and metamorphism in the MCT zone and Tibetan slab, eastern Himalaya, *Tectonics*, *8*, 865–880, 1990.

Isacks, B.L., and M. Barazangi, Geometry of Benioff zones: Lateral segmentation and downwards bending of the subducted lithosphere, in *Island Arcs, Deep Sea Trenches,*

and Back-Arc Basins, Maurice Ewing Series 1 Edited by M. Talwani and W.C. Pitman III, 99–114, A. G. U. Washington D.C., 1977.

Ishida, M., and A.K. Hasemi, Three-dimensional fine velocity structure and hypocentral distribution of earthquakes beneath the Kanto-Tokai district, Japan, *J. Geophys. Res.*, *93*, 2076–2094, 1988.

Johnson, M.R.W., The structural evolution of the Kumaon Lesser Himalaya, in *Current trends in Geology IX, Himalayan Thrust and Associated Rocks* Edited by P. S. Saklani, 27–39, 1986.

Lachenbruch, A.H., and J.H. Sass, Thermo-mechanical aspects of the San Andreas fault system, in *Proceedings of the Conference on Tectonic Problems of the San Andreas Fault System* Edited by R.L. Kovach and A.Nur, pp. 192–205, School of Earth Sciences, Stanford University, Stanford, Calif., 1973.

Lachenbruch, A.H., and J.H. Sass, Heat flow and energetics of the San Andreas fault zone, *J. Geophys. Res.*, *85*, 6185–6222, 1980.

Le Fort, P., Himalayas: the collided range. Present knowledge of the continental arc, *Am. J. Sci.*, *275A*, 1–44, 1975.

Le Fort, P., Manaslu leucogranite: A collision signature of the Himalaya. A model for its genesis and emplacement, *J. Geophys. Res.*, *86*, 10545–10568, 1981.

Le Fort, P., Metamorphism and magmatism during the Himalayan collision, in *Collision Tectonics, Spec. Publ. 19* Edited by M.P. Coward and A.C. Ries, 159–172 Geol. Soc. London., 1986.

Le Fort, P., Granites in the tectonic evolution of the Himalaya, Karakorum and southern Tibet., *Philosoph. Trans. R. Soc. Lond. Ser. A* , *326*, 281–298, 1988.

Le Fort, P., M. Cuney, C. Deniel, C. France-Lanord S.M.F. Sheppard, B.N. Upreti and P. Vidal, Crustal generation of the Himalayan leucogranites, *Tectonophysics*, *134*, 39–57, 1987.

Lyon-Caen, H., and P. Molnar, Gravity anomalies, flexure of the Indian plate, and the structure, support and evolution of the Himalaya and Ganges Basin, *Tectonics*, *4*, 513–538, 1985.

McGarr, A., Some constraints on levels of shear stress in the crust from obsevations and theory., *J. Geophys. Res.*, *85*, 6231–6238, 1980.

McKenzie, D., and G. Jarvis, The conversion of heat into mechanical work by mantle convection, *J. Geophys. Res.*, *85*, 6093–6096, 1980.

Meissner, R., and J. Strelau, Limits of stresses in continental crusts and their relation to the depth-frequency distribution of shallow earthquakes., *Tectonics*, *1*, 73–90, 1982.

Minster, J. B., and T. H. Jordan, Present-day plate motions, *J. Geophys. Res.*, *83*, 5331–5354, 1978.

Molnar, P., and H. Lyon-Caen, Fault plane solutions of earthquakes and active tectonics of the Tibetan plateau and its margins, *Geophys. J.*, *99*, 123–153, 1989.

Molnar, P., W.-P. Chen, and E. Padovani, Calculated temperatures in overthrust terrains and possible combinations of heat sources responsible for the Tertiary granites in the Greater Himalaya, *J. Geophys. Res.*, *88*, 6415–6429, 1983.

Mount, V.S., and J. Suppe, State of stress near the San Andreas fault: implications for wrench tectonics, *Geology*, *15*, 1143–1146, 1987.

Ni, J., and M. Barazangi, Seismotectonics of the Himalayan collision zone: Geometry of underthrusting of Indian plate beneath the Himalaya, *J. Geophys. Res.*, *89*, 1147–1164, 1984.

Obara, K., and H. Sato, Existence of an S-wave reflector near the upper plane of the double seismic zone beneath the southern Kanto district, Japan, *J. Geophys. Res.*, *93*, 15037–15045, 1988.

Olgaard, D.L., and W.F. Brace, The microstructure of gouge from a mining-induced seismic shear zone., *Int. J. Rock Mech. Mineral. Sci. Geomech. Abstr.*, *20*, 11–19, 1983.

O'Niel, J.R., and T. C. Hanks, Geochemical evidence for water-rock interaction along the San Andreas and Garlock faults, California, *J. Geophys. Res.*, *85*, 6286–6292, 1980.

Oxburgh, E.R., and D.L. Turcotte, Thermal structure of Island Arcs, *Geol. Soc. Am. Bull.*, *81*, 1665-1688, 1970.

Oxburgh, E.R., and D.L. Turcotte, Thermal gradients and regional metamorphism in overthrust terrains with special reference to the Eastern Alps, *Schweiz. Mineral. Petrogr. Mitt.*, *54*, 641–662, 1974.

Parsons, B., and J. G. Sclater, An analysis of the variation of ocean floor bathymetry and heat flow with age, *J. Geophys. Res.*, *82*, 803-827, 1977.

Press, W.H., B.P. Flannery, S.A. Teukolsky and W.T. Vetterling, *Numerical Recipes*, 818pp Cambridge University Press, New York, 1986.

Rao, R.U.M., G.V. Rao, and H. Narain, Radioactive heat generation and heat flow in the Indian shield, *Earth Planet. Sci. Lett.*, *30*, 57–64, 1976.

Ruppel, C., L. Royden, and K.V. Hodges, Thermal modeling of extnsional tectonics: Application to pressure-temperature-time histories of metamorphic rocks, Tectonics, *7*, *947–957*, 1988.

Scholz, C.H., Shear heating and the state of stress on faults, *J. Geophys. Res.*, *85*, 6174–6184, 1980.

Scholz, C.H., J. Beavan, and T.C. Hanks, Frictional metamorphism, argon depletion, and tectonic stress on the Alpine fault, New Zealand, *J. Geophys. Res.*, *84*, 6770–6882, 1979.

Schwartz, S.Y., J.W. Dewey, and T. Lay, Influence of fault plane heterogeneity on the seismic behavior in the southern Kurile islands arc, *J. Geophys. Res.*, *94*, 5637–5699, 1989.

Seno, T., and T. Takano, Seismo-tectonics at the trench-trench-trench triple junction off central Honshu, *Pure and Appl. Geophys.*, *129*, 27–40, 1989.

Sibson, R.H., Power dissipation and stress levels on faults in the upper crust, *J. Geophys. Res.*, *85*, 6239–6247, 1980.

Sibson, R.H., Fault zone models, heat flow and depth distribution of earthquakes in the continental crust of the United States, *Bull. Seismol. Soc. Am.*, *72*, 151–163, 1982.

Tapponnier, P., and P. Molnar, Slip-line field theory and large scale continental tectonics, *Nature*, *294*, 319–324, 1976.

Toksöz, M.N., J.W. Minear, and B.R. Julian, Temperature fields and geophysical effects of a downgoing slab, *J. Geophys. Res.*, *76*, 1113–1138, 1971.

Turcotte, D.L., and G. Schubert, Frictional heating of the descending lithosphere, *J. Geophys. Res.*, *78*, 5876–5886, 1973.

Uyeda, S., and K. Horai, Terrestrial heat flow in Japan, *J. Geophys. Res.*, *69*, 2121–2141, 1964.

Valdiya, K.S., The two intracrustal boundary thrusts of the Himalaya, *Tectonophysics*, *66*, 323–348, 1980.

Vidal, P., A. Cocherie, and P. Le Fort, Geochemical investigations of the origin of the Manaslu leucogranite (Himalaya, Nepal), *Geochim. Cosmochim. Acta*, *46*, 2279–2292, 1982.

Watanabe, T., M.G. Langseth, and R.L. Anderson, Heat

flow in back-arc basins of the western Pacific, in *Island Arcs, Deep Sea Trenches, and Back-Arc Basins, Maurice Ewing Series 1* Edited by M. Talwani and W.C. Pitman III, 137–161 Am. Geophys. U. Washington D.C., 1977.

Zoback, M.D., M.L. Zoback, V.S. Mount, J. Suppe et al., New evidence on the state of stress of the San Andreas fault system, *Science, 238*, 1105–1111, 1987.

P. England, Department of Earth Sciences, Oxford University, Parks Road, Oxford OX1 3PR, England.

P. Molnar, Department of Earth, Atmosphere and Planetary Sciences, Massachusetts Institute of Technology, Cambridge, MA 02139.

(Received May 30, 1989;
revised September 14, 1989;
accepted September 29, 1989.)